Praca wykonana w ramach projektu TEAM kierowanego przez Prof. Pawła Moskala. Projekt finansowany przez Fundację na rzecz Nauki Polskiej.

This work is supported by the Foundation for Polish Science under Grant TEAM/2017-4/39

Jagiellonian Univeristy
Faculty of Physics, Astronomy and Applied Computer Science

Marian Smoluchowski Institute of Physics
Experimental Physics within Studies in Mathematics and Natural Sciences

Szymon Parzych

Album number: 1134340

Study of the Total Body J-PET sensitivity with the Toy Monte-Carlo model

Master thesis
Field of study: Experimental Physics within Studies in Mathematics and Natural Sciences

Supervisor:
prof. dr hab. Paweł Moskal
Department of Experimental
Particle Physics and Applications

Kraków 2021

Acknowledgments

I would like to express my deepest gratitude to all people without whom this thesis would not have been possible.
First of all, I would like to thank my supervisor prof. dr hab. Paweł Moskal for giving me the opportunity to work in his research group, for his guidance, help and encouragement.
Moreover, I am grateful to dr Michał Silarski, my Bachelor thesis supervisor, who introduced me into the scientific life and confirm my conviction in such career choice.
I want to thank dr Szymon Niedźwiecki for teaching me the laboratory part of experimental physicist work.
I also thank the whole J-PET team for a friendly atmosphere and lots of fruitfull discussions. Special thanks to Meysam Dadgar and Faranak Tayefi Ardebili for not only countless hours of talks, problem solving and other divagations but mostly for the friendship, which goes beyond the work.
Last but not least, I would like to thank my parents, sister and rest of the family for love, patience and always believing in me.

Abstract

The main aim of presented thesis is to investigate sensitivity of the Total Body J-PET scanners as a function of their axial field of view and inner module construction, as well as assessing the influence of the angular acceptance criterion (used for PET performance optimization) on this characteristic. In order to achieve this goal a simulation-based study was carried out with a use of the standard Monte-Carlo simulation software – Geant4 Application for Tomography Emission (GATE). Moreover, a Toy Monte-Carlo model has been developed as a simplified approach to the sensitivity investigation. Its principle of operation, as well as detailed validation by comparison with GATE software is presented in this work. The obtained results demonstrate that the standard imaging total sensitivity achievable with the Total Body J-PET scanners equals to 25.92(05±04) [cps/kBq] for the 2 meter long two-layer tomograph and 84.74(0.9±1.1) [cps/kBq] for the 2.5 meter long four-layer tomograph. Such results exceed the conventional PET systems (represented by the Biograph Vision) by a factor of ~ 4.5 and ~ 15 respectively. At the same time sensitivity at the center of the tomograph can reach up to 124.1(1.0±1.1) [cps/kBq]. Furthermore, due to the possibility of the positronium mean lifetime imaging guaranteed by the J-PET technology, its sensitivity based on the triple γ coincidence technique has been evaluated. The acquired maximal total sensitivity of 30.63(06±31) [cps/kBq] proves to again surpass the traditional crystal-based system up to ~ 5 times. Ultimately, the sensitivity achieved with the studied Total Body scanners is almost uniform along the whole patient with an additional increase on its sides for both double and triple coincidence imaging. This creates a possibility for high-quality simultaneous imaging of the whole human body.

Streszczenie

Głównym celem przedstawianej przeze mnie pracy jest zbadanie wydajności skanerów Total Body J-PET w funkcji ich długości oraz wewnętrznej konstrukcji modułów, jak również zbadania wpływu kryterium akceptancji kątowej (używanej do optymalizacji działania skanera PET) na ten parametr. W tym celu przeprowadzono oparte na symulacjach badania z wykorzystaniem standardowego oprogramowania do symulacji Monte-Carlo — Geant4 Application for Tomography Emission (GATE). Ponadto opracowano model Toy Monte-Carlo jako uproszone podejście do zagadnienia badań wydajności tomografów. Jego zasada działania, a także szczegółowa walidacja poprzez porównanie z oprogramowaniem GATE została zaprezentowana w tejże pracy. Otrzymane wyniki pokazują, że całkowite wydajności standardowego obrazowania osiągalne z tomografami Total Body J-PET wynoszą odpowiednio 25.92(05±04) [cps/kBq] dla dwumetrowego, dwuwarstwowego skanera i 84.74(0.9±1.1) [cps/kBq] dla dwuipółmetrowego, czterowarstwowego skanera. Tym samym przewyższają one wyniki dla konwencjonalnych systemów PET (reprezentowanych przez Biograph Vision) odpowiednio o czynnik ~ 4.5 i ~ 15. Jednocześnie wydajność w centrum tomografu może osiągnąć aż do 124.1(1.0±1.1) [cps/kBq]. Ze względu na możliwość obrazowania na podstawie średniego czasu życia pozytronów gwarantowanego przez technologię J-PET, została wyznaczona odpowiadająca mu wydajność bazująca na technice potrójnej koincydencji fotonów. Maksymalna otrzymana całkowita wydajność równa 30.63(06±31) [cps/kBq] do 5 razy przewyższa wyniki dla konwencjonalnych skanerów zbudowanych z kryształów. Uzyskana dla badanych tomografów wydajność jest niemal jednolita wzdłuż całego ciała pacjenta z dodatkowym wzrostem przy jego końcach, zarówno dla techniki podwójnej jak i potrójnej koincydencji. Zapewnia ona możliwość jednoczesnego obrazowania całego człowieka z wysoką jakością.

Contents

1 Introduction

The aim of the thesis is to investigate the sensitivity of the introduced by the J-PET Collaboration Total Body scanners [1, 2, 3, 4]. This goal is achieved through a simulation-based study carried out with a standard software for Monte-Carlo simulations and a Toy Monte-Carlo software developed in the framework of this thesis.

According to World Health Organization report [5] tumors, called in their malignant versions – cancers, are the leading cause of death alongside the cardiovascular diseases. Cancer is estimated to be responsible for one in six deaths globally [5]. Since many cancers cannot be yet prevented, treatment is the only available alternative, and early diagnosis is the key to its success. In the worst case, it allows to either extend a person's life or to manage the symptoms and pain.

There are many methods for the diagnosis of tumors such as Medical Ultrasound, Computer Tomography (CT), Magnetic Resonance Imaging (MRI), Mammography or Positron Emission Tomography (PET). CT and MRI enable determination of anatomical and morphological images of a human, while PET provides alternative information about its metabolism. Researchers are constantly improving and developing PET technology to make PET imaging more precise and accessible for people. One of the relatively new and popular trends in the medical imaging techniques are the construction of Total Body PET tomographs [6]. Thanks to a whole human body coverage such systems are many times more efficient and accurate than standard clinically available PETs of length up to 26 cm [7]. However, one of their main disadvantages is their price due to the use of enormous amount of electronics and detectors. Therefore, it is imperative to look for a new Total Body PET designs in order to introduce them into common clinical practise.

At the Jagiellonian University in Cracow, Poland, an international group of researchers called Jagiellonian PET Collaboration (J-PET) is developing a novel Total Body PET system. Thanks to the application of plastic scintillators for detectors and their axial arrangement, it may present in the future an advanced, precise and cost-effective PET tomograph practicable for the common clinical introduction [1, 2, 3, 4].

Despite the obvious importance of Positron Emission Tomography in medicine like medical diagnostics or treatment monitoring, PET tomograph is also a perfect system for many fundamental physics research [8]. Creation of quasi-stable bound state of electron and positron called positronium even during standard imaging session can be used to perform tests of discrete symmetries in the leptonic object via the determination of the expectation values of the discrete symmetries odd operators. Moreover, it enables test of quantum entanglement [4, 8, 9, 10].

Development of any new tomograph always starts with multitude of computer simulations aiming to decide about its effectiveness. Among parameters usually taken into account, the sensitivity is one of the most important as it is responsible for the amount of collected data, which can be then used for creation of a patient image. The standard approach to such simulations is based on the advanced softwares for Monte-Carlo simulations like GATE [11, 12, 13, 14] or Geant4 [15, 16, 17]. However, the proper use of them requires training and is time-consuming. In this work I introduce a developed simplified approach to the investigation of sensitivity of PET scanners by the use of Toy Monte-Carlo model and compare its results with the GATE software. Moreover, I present its applicability and perform a study of Total Body PET tomographs proposed by the J-PET Collaboration.

This thesis is divided into eight chapters. Second chapter gives a description of Positron Emission Tomography's principle of operation and the way to construction of a Total Body PET systems. The third chapter has been dedicated to the introduction of J-PET innovative technology in the construction of tomographs. The fourth chapter presents a study of the Total Body J-PET systems sensitivity using the GATE software. The description of introduced in this thesis Toy Monte-Carlo model, together with its validation is provided in chapter 5. Chapter 6 concerns the sensitivity results of J-PET technology tomographs with a use of presented Toy Monte-Carlo technique. Chapter 7 is devoted to the studies of the positronium imaging sensitivity that requires triple coincidence technique connecting standard back-to-back gamma registration with registration of prompt photons. The final, eighth chapter includes summary and conclusions.

2 Positron Emission Tomography PET

Positron Emission Tomography (PET) is one of the most technologically advanced diagnostic methods which provides non-invasive imaging of ongoing physiological processes in the body. It plays a fundamental role both in medical diagnostics, as well as in monitoring of effects of therapy in oncology, cardiology and neurology. PET allows to determine the spatial and temporal distribution of concentration of selected substances in the body. To take advantage of this possibility, the patient is administered pharmaceuticals marked with radioactive isotope emitting positrons. Difference in rate of assimilation of such pharmaceuticals inside various tissues allows to identify sections of the diseased cells with high accuracy. This method is proven to be highly effective in particular in locating and diagnosing of cancer metastasis [18, 19, 20, 21].

In order for the idea of PET tomography to emerge, many important discoveries had to be made. The discovery of the positron, invention of the cyclotron, recognition that the radionuclides such as ^{11}C, ^{13}N, ^{15}O or ^{18}F were important for the tracing of important biochemical pathways and invention of the scintillation detector dates back to the time period of late 1920s up to late 1940s. Thanks to them, first concepts of positron emission tomography were created in 1950s and first tomographs with clinical uses in 1970s. In the list of creators there are names such as David E. Kuhl, Roy Edwards, Michel Ter-Pogossian, Michael E. Phelps, Edward J. Hoffman and many others [22, 23, 24].

2.1 Principle of operation

The principle of operation of positron emission tomography lies in the detection of pairs of two, back-to-back photons. In order to create such pairs, patient is administered radiopharmaceutic which consists of two substances: ligand and radioactive isotope. Ligand is a molecular structure that transfers radioisotope and accumulate in the imaged organ or tissue. It is selected with knowledge about the target site. Its molecules can directly interact with tissue and cells or take part in metabolic processes. Radioactive isotope, thanks to its short half-life time and $\beta+$ decay channel provides positrons necessary for creation of photons in the annihilation process with electrons. Radionuclides are produced in accelerators by bombarding targets with charged projectiles like protons, deuterium or α particles. One of the commonly used radioisotopes in PET scans is ^{18}F which together with glucose creates ^{18}F-Fluorodeoxyglucose (FDG) used for tracking tissue metabolism in the body [19, 20, 21, 25].

Positron emission and annihilation

During $\beta+$ decay process radioactive nuclide decays by converting proton to a neutron with emission of a positron and an electron neutrino. On the nuclear level this process can be described as:

$$^{A}_{Z}X \rightarrow {}^{A}_{Z-1}Y + e^{+} + \nu_e,$$

where A is a mass number, Z - atomic number, X - initial element, Y - final element, e^+ - positron and ν_e is an electron neutrino. Once created, the positron travels a certain distance, losing its kinetic energy mainly by interactions with encountered electrons. When its energy drops below 10 keV the positron can immediately annihilate with the electron with creation of two photons emitted approximately 180° apart with energy of 511 keV each or create an unstable state called positronium [19, 20, 21, 25]. The positronium (Ps) can exist in two states:

- Singlet state $^1S_0$ called para-positronium (p-Ps) with spin equal to 0 and mean lifetime in vacuum equal to 0.125 ns,
- Triplet state $^3S_1$ called ortho-positronium (o-Ps) with spin equal to 1 and mean lifetime in vacuum equal to 142 ns.

Due to the symmetry of charge conjugation, p-Ps undergoes annihilation with emission of an even number of photons (most often two, back-to-back), while o-Ps undergoes annihilation with emission of an odd number of photons (most often three) [8].

Interaction of annihilation photons with matter and their detection
For the purpose of positron emission tomography only the events which resulted in creation of the pair of gammas are taken into account. The photoelectric effect and Compton effect (Compton scattering) are two major mechanisms by which 511 keV photons interact with matter. In the first one, photon interacts with an electron ejecting it from the inner shell of an atom. Such electron is then called photoelectron. This can be followed by transfer of an electron from higher to lower energy shell which results in a photon emission. In the second type, photon transfers part of its energy to loosely bound electron in the medium, ejects it and changes the direction of flight (scatter) [19, 20, 21, 25, 26].

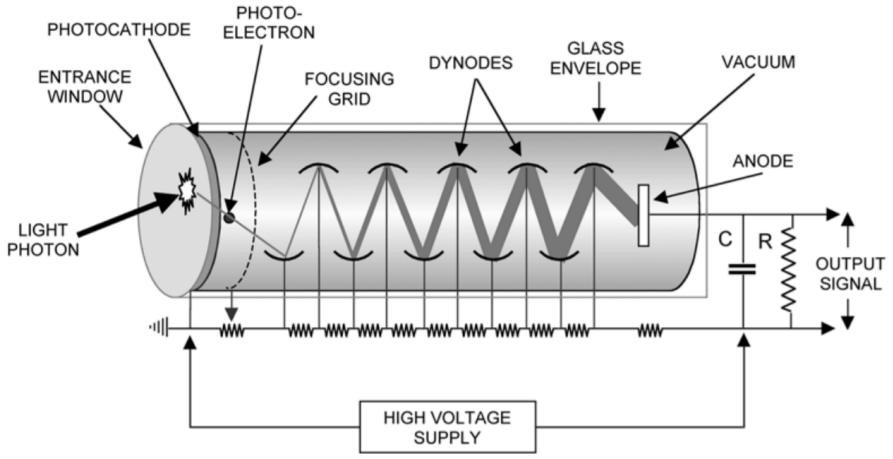

Figure 1: A photomultiplier tube consists mainly of a photocathode, a series of dynodes (electrodes) each of which is held at a greater voltage and an anode. Light photons striking the photocathode can release electrons into the tube which are then accelerated and multiplied on the dynodes to finally be turned into an electrical signal [20].

The most common type of the detector used in present PET systems is the scintillator detector. Such detector consist of a dense scintillator (usually a crystal [7, 20, 21]) that serves as an interacting medium for the gammas created in the annihilation and of a photomultiplier. Electrons knocked out from scintillator material in the above-mentioned processes ionize another atoms, which then de-excitate with emission of new photons. Light from the scintillator excites the photocathode placed on one side of the photomultiplier tube (see Figure 1) and liberate so-called photoelectrons. Photoelectrons are then focused to the first dynode and thanks to increasing voltage, accelerated and multiplied while passing to the next ones. Finally they reach the anode and are converted into an electrical signal [19, 20, 21, 26].

Coincidence detection and image reconstruction

The most popular types of PET tomographs have a cylinder-like geometry with a large number of radially arranged detectors. When annihilation occurs somewhere inside of this cylinder, each of the emitted photons can interact with one of the detectors. If both of them will be registered, one can deduce that annihilation occurred somewhere along the line connecting the two detectors. Such line is usually called a Line Of Response (LOR). To reconstruct the density distribution of the points where the annihilation occurred, data from a large number of LORs is collected at different angles and radial offsets [20].

The registration process is done using the coincidence detection technique. Not only do photons need to deposit enough energy into the detectors to meet energy window criteria, but they also have to do it within a certain time window in order to be assigned to the same event.

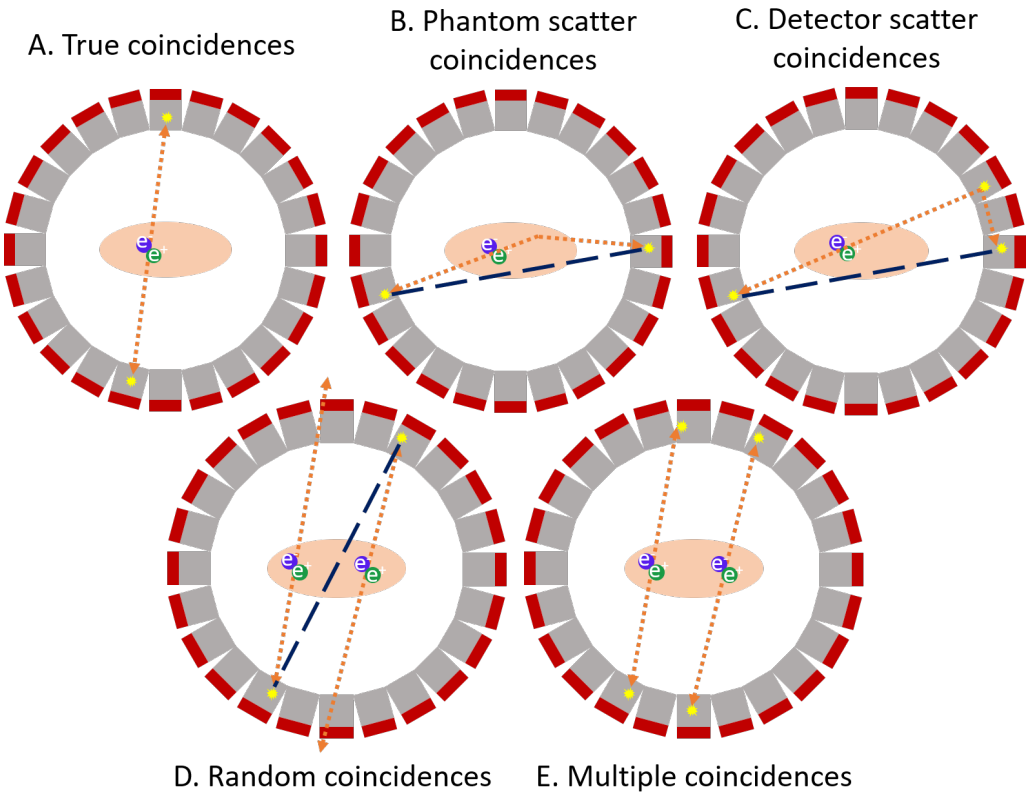

Figure 2: Illustration of the five main coincidence event types: A – True coincidence, B – Phantom scattered coincidence, C – Detector scattered coincidence, D – Random coincidence and E – Multiple coincidence. Each of the figures show a transaxial view of the ring of detectors with the patient inside. The annihilation points are marked with blue (electron) and green (positron) circles, the annihilation photons with orange arrows, places of interaction with yellow stars and the incorrect LORs with black dashed lines.

In the ideal case, only true coincidences (see Figure 2.A.) would be recorded. This name refers to the events where the two detected photons originate from the same annihilation and their direction of flight wasn't changed before detection. However, in reality one can also record unwanted random, scattered and multiple coincidences [19, 20, 21, 27]:

- Scatter coincidences happen when one or both of the two annihilation photons have undergone a Compton scatter interaction (either inside the patient's body or within

the scintillator material) and changed direction before final registration (see Figure 2.B. & Figure 2.C.).

- Random (or accidental) coincidences occur when two registered γ quanta originate from unrelated events (see Figure 2.D.).
- Multiple coincidences occur when three or more photons are detected simultaneously (see Figure 2.E.).

In most of the cases only one of the two annihilation photons is detected. This happens when second one is depositing insufficient energy, doesn't interact with the detector, or is on a trajectory that does not intersect with any detector. Such events play a significant part in the undesirable coincidences. All three of the above types of unwanted coincidences have a degrading effect on the measurement and need to be corrected to obtain an image that represents as closely as possible the actual concentration of radioactivity [20].

2.2 Sensitivity

Mechanical construction of a new PET scanners is usually preceded by multitude of computer simulations in order to determine the quality and usefulness of the design. One of the factors determining quality in context of the final image is the number of coincidence events that can be detected. This number is dictated by the amount of injected radioactivity, the fraction of activity that reaches the tissues of interest, the imaging time, and the sensitivity of the PET system. However, due to limits set for the amount of administered radioactivity and the imaging time, sensitivity is the key to improving the image quality. Because of that, it is one of the most important parameters taken into account while designing new Positron Emission Tomographs.

The sensitivity of a scanner is defined as the rate of true coincidence events detected by the device for each unit of activity present in the radioactive source, expressed either in counts per second per microcurie ($cps/\mu Ci$) or in count per second per becquerel (cps/Bq). It depends on factors such as the efficiency of the detectors for registering the 511 keV photons, the solid angle coverage of the scanner, the location of the radioactivity with respect to the tomograph, and the time and energy windows applied to the collected data [7, 20].

Guidelines for performance measurements of Poistron Emission Tomographs including their sensitivity are standardized, gather and published by the National Electrical Manufacturers Association (NEMA) [28]. The latest collection of rules was published in "NEMA Standards Publication NU 2-2018" in 2018. According to them, there are two parameters that should be reported for sensitivity measurement: the system (total) sensitivity and the sensitivity profile. The first one denotes the ratio of rate of true coincidence registrations in tomograph to the total activity of the source:

$$S_{tot} = \frac{R}{A} \ . \tag{1}$$

The sensitivity profile represents the dependence of sensitivity of the detection of the source on the axial positioning of it (see Figure 3). It usually takes form of a histogram, where each bin (slice) corresponds to sensitivity S_i of appropriate fraction of the source:

$$S_i = \frac{R_i}{A_i} \ , \tag{2}$$

where R_i represents rate of registered true coincidences originating within the slice i and A_i is a fraction of activity located in it. The characteristic triangular-like shape of the

profile comes from the decreasing symmetric angular coverage of the source together with its increasing displacement from the center. Smaller symmetric angular coverage decreases possibility of back-to-back photons flight path overlap with the detectors.

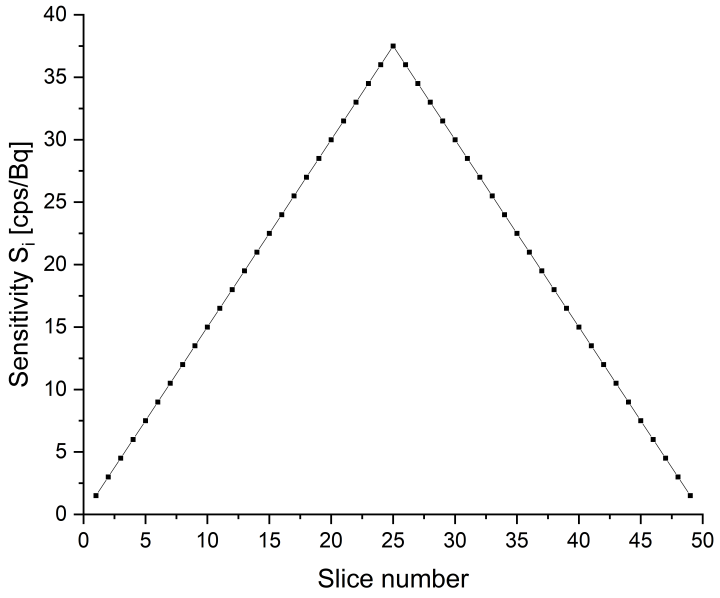

Figure 3: Exemplary sensitivity profile for a system divided into 49 slices in the longitudinal direction.

The use of standardized NEMA guidelines allows for simple quality checks and comparison of PET tomographs. Nevertheless, described in them sensitivity comes from the limit of attenuation free measurement. While from the Monte-Carlo simulation point of view this is simple to achieve (with a use of back-to-back source instead of positron emitting source), this parameter does not show the number of events taking into image reconstruction while source, in a form of radiopharmaceutic, is administered to a patient. Therefore, I introduced an additional sensitivity definition as a ratio of the number of events utilized for the image reconstruction (only true coincidences) to the number of all events created within the human body (defined by the source activity) for measurements performed with a patient or phantom. The sensitivity defined in this way allows for the estimation of how many of events interesting from the point of image reconstruction can the PET system detect while performing real imaging session on a patient. Consequently, there is a need for redefinition of system (total) sensitivity and sensitivity profile (based on slice i sensitivity):

$$S_{tot}^{ph} = \frac{R^{ph}}{A^{ph}} \ , \tag{3}$$

$$S_{i}^{ph} = \frac{R_{i}^{ph}}{A_{i}} \ , \tag{4}$$

where R^{ph} denotes rate of only true coincidence registrations (omitting phantom scattered coincidences), R_i^{ph} represents respective rate of the ones originating within the i-th slice and A^{ph} corresponds to the total activity located in the phantom region.

2.3 From PET to Total Body PET scanners

In the initial years PET tomographs were based on different geometries, for example rotating partial ring systems or flat panel detectors. The axial field of view (AFOV) of such systems was not longer than 30 cm, which was sufficient for a brain or cardiac PET scans. There were some prototypes with an axial field of view longer than 50 cm but they were not introduced into common practice [29, 30]. Nowadays, the vast majority of PET tomographs consists of a full ring of radially arranged detectors. However, the standard axial length of a ring still ranges from 15–26 cm. Within such short field of view, the imaging system contains only a small part of the human body and is good for only single organ scans. For applications in which the distribution of the radiopharmaceutic in the whole human body or multiple organ imaging is of interest, this length is insufficient [7, 6].

A solution for that problem was provided in the, so-called, whole-body PET system (see Figure 4.A.). In this tomograph, the axial FOV remains the same as in classic PET, but the difference lies in the possibility of bed translation. Because of that, one can scan the entire human body part by part. There are two modes in which this system can work. First one is a step and shoot mode. The operator makes few scans of different parts of the body thanks to changing bed position and then add results. Second one is very similar but with a continuous bed movement instead of the discrete steps. Unfortunately, even on today's best scanners the total sensitivity of detection of annihilation photon pairs is under 1% [7]. There are two major factors contributing to this result. Firstly, at any one time most of the body is outside the FOV of the scanner and no true coincidences can be detected. Secondly, even for the organ inside the field of view only small percentage of photons can be detected due to their isotropic radiation [6].

Both factors are addressed by covering the entire human body with multiple detector rings. This concept is called Total Body PET (see Figure 4.B.). From approximate computer simulations it turns out, that extending PET tomograph up to 200 cm of axial field of view will improve total sensitivity several dozen times, and one organ imaging sensitivity several times [6]. Another advantage is that the time of scan with a Total Body PET (TB PET) is decreased in comparison to a whole-body PET due to the simultaneous imaging of the whole human body. Moreover, there are other positive consequences which comes from gain in sensitivity. Firstly, the sensitivity gain can be used to increase the signal-to-noise ratio (SNR) in the reconstructed image in comparison to classic PET SNR. Secondly, one can sacrifice this gain in order to reduce the time of the scan even more, while maintaining the SNR at classic level. The entire scan could then be completed in less than one minute instead of 10-20 minutes. It opens possibility to single-breath-hold PET imaging and improves image quality due to reduction of patient motion. Another option would be to use the sensitivity gain to reduce the number of activity injected with the radiopharmaceutical. Finally, it also allows for longer tracing time of the radiotracer substance, which is especially useful when it comes to short-lived radionuclides. It can extend time between creation of the radiopharmaceutical and administration of it to the patient [6].

Total Body projects

The concept of PET scanners with a long axial field of view is not new. There were at least two prototypes created in the first decade of this century with length over 50 cm. One of them was developed by Hamamatsu using BGO crystals and had an axial length of 68.5 cm [29]. The second system was developed by Siemens using LSO crystals with 53 cm AFOV [30]. However, many drawbacks of both tomographs prevented their commercialization [6, 31]. There are currently at least four groups actively working on Total

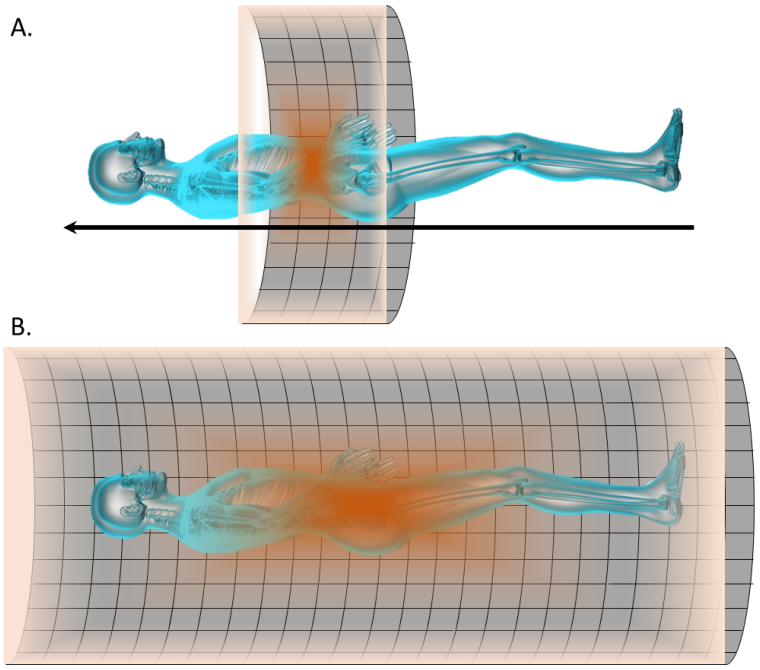

Figure 4: Scheme of the whole-body PET (A) and Total Body PET (B) solution to the problem of imaging of the whole human body, together with symbolic sensitivity of the tomograph (marked with orange gradient). The first one operates on the principle of patient movement through the standard PET system, while the second one allows for imaging in only single position.

Body PET tomographs: the EXPLORER Consortium from the UC Davis in California, United States of America [32], the Siemens Healthineers [33], the PET2020 from the Ghent University, Belgium [34, 35] and the Jagiellonian PET Collaboration from the Jagiellonian University in Cracow, Poland [1, 2, 3, 4].

EXPLORER PET Consortium
Led by the University of California, Davis (UC Davis), the EXPLORER Consortium includes researchers from the University of Pennsylvania and Lawrence Berkeley National Laboratory. Currently their are working on at least two Total Body solutions. First of them is the PennPET Explorer whole-body scanner developed by the University of Pennsylvania team in collaboration with KAGE Medical and Philips. It uses lutetium-yttrium oxyorthosilicate (LYSO) scintillation crystals, each coupled to the digital silicon photomultiplier sensor. For the time being system consists of 3 rings of radially arranged crystals operational with an active 64 cm axial FOV, with plans of expanding it to 140 cm [6, 36, 37, 38]. Second one, developed by the UC Davis and United Imaging Healthcare, is the uEXPLORER. This TB PET system uses 8 rings of LYSO scintillation crystals read out by silicon photomultipliers (SiPMs) and has a total of 194.8 cm field of view. It became operational in the mid-2018 [6, 7, 36].

Siemens Healthineers
Siemens Healthineers AG is the mother company for several medical technology companies and is headquartered in Erlangen, Germany. Siemens Healthineers is connected to the

larger corporation, Siemens AG. In 2020 they introduced a new PET tomograph called "Biograph Vision Quadra". With 106 cm axial PET field of view, it ensures a vertex to thighs perspective. This system uses the $3.2 \times 3.2 \times 20$ mm LSO crystals coupled with SiPM detector and time-of-flight performance [33].

PET2020
This group from the Ghent University is developing a PET scanner consisting of $50 \times 50 \times 16$ mm monolithic LYSO crystals with an adaptive axial FOV of length up to 2 meters and 65 cm inner diameter [34, 35].

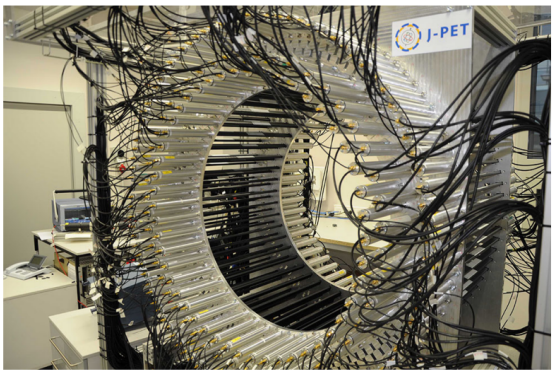

(a) Photo of the PET tomograph prototype constisting of 192 plastic scintillator strips arranged in three layers [1, 2, 3, 4].

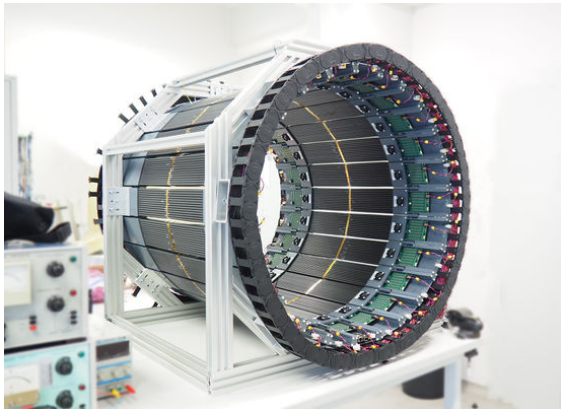

(b) Photo of the Modular PET tomograph prototype constisting of 24 modules of plastic scintillator strips [1, 2, 3, 4].

Figure 5: Photos of the 2 prototypes of PET scanners developed by the J-PET Collaboration.

Jagiellonian PET Collaboration
It is an interdisciplinary and international group including researchers from the Jagiellonian University, National Centre for Nuclear Research, Maria Curie-Skłodowska University, University of Vienna, National Laboratory in Frascati and from the companies Nowoczesna Elektronika and Brain Waves Electronics [4]. The Jagiellonian PET (J-PET) Collaboration proposes a novel, cost-effective approach to PET tomographs with a use of axially arranged plastic strips as scintillator detectors.

There are currently 2 prototypes of the J-PET scanner, both with 50 cm long AFOV. One of them consists of 192 plastic strips arranged in three layers, which form a cylinder with the inner diameter of 85 cm (see Figure 5a). Each scintillator is read out by two silicon photomultipliers located at the ends of the strip. Second one is the Modular J-PET build out of 24 detection modules (see Figure 5b). Each module is an independent detection unit weighting 2 kg which consists of 13 plastic scintillator strips read out at both sides by matrices of SiPMs and can be easily taken out of the scanner. Such construction allows for simple transportation, assembly and disassembly of tomograph with any number of modules [4, 2, 39].

Moreover, the Total Body J-PET scanner is under a research. The structure of such tomograph would be similar to the Modular J-PET but with several times longer axial FOV. Since plastic scintillators are much less expensive than inorganic crystals and readouts are placed at the both ends of the strips so they total number while lengthening wouldn't change, such scanner would be an economic alternative for the crystal TB PETs [1, 3].

3 Jagiellonian Positron Emission Tomograph J-PET

A novel PET system called J-PET (Jagiellonian Positron Emission Tomograph) is being developed at the Jagiellonian University in Cracow by the J-PET Collaboration. The novelty of this tomograph lies in the usage of axially arranged plastic strips as scintillator detectors in contrast to the conventional PET scanners, which are based on radially arranged inorganic crystal scintillators [7, 18, 20, 21]. By replacing a row of crystals along the longitudinal axis of a tomograph with one plastic strip, structure and construction of the J-PET scanner is becoming much simpler. Moreover, each strip is read out by silicon photomultipliers located at both ends, while in traditional case the scintillators are read out from one side. Such approach allows not only for lowering the price by usage of fewer and cheaper scintillators but also by reducing amount of needed electronics [1, 2, 4].

While currently there are 2 prototypes of the J-PET scanner (see Figure 5), both with 50 cm long AFOV, presented structure allows for conversion to Total Body PET. It can be introduced either as assemblage of few half meter long scanners (as it is done in case of conventional PET systems) or by exchanging 50 cm long scintillator strips with longer ones. Furthermore, usage of proposed modular system (described in the *Jagiellonian PET Collaboration* paragraph in chapter 2.3) allows for simple montage of tomograph with any number of modules enabling examination of patients who cannot be examined with the conventional PET due to factors such as obesity or claustrophobia [1].

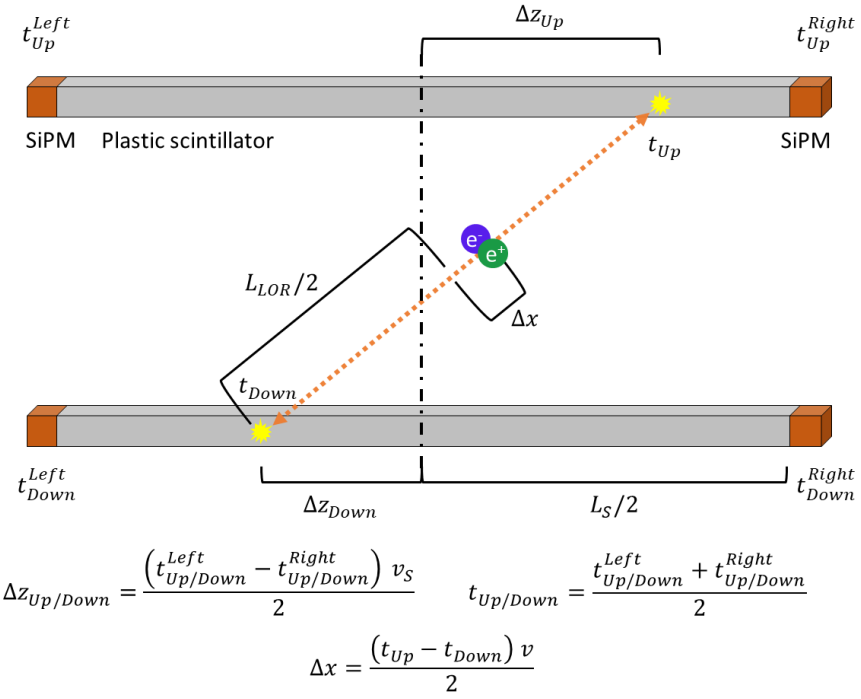

Figure 6: Illustration of the annihilation position analysis for J-PET technology PET tomographs based on the time of flight measurements. Important markings: L_S – length of the plastic scintillator strip; L_{LOR} – length of the line of response; Δx – displacement of annihilation point from the center of the LOR; $\Delta z_{Up/Down}$ – displacement of the hit 'z' coordinate from the scintillator center; $t_{Up/Down}^{Left/Right}$ – time of signal arrival to SiPM; $t_{Up/Down}$ – time of gamma interaction with scintillator material.

In presented solution of PET tomograph build from long scintillator strips the knowledge of annihillation position is provided by the time of flight (TOF) measurements as illustrated in Figure 6. The location of each hit within the scintillator material can be reconstructed based on the difference between time of signal on respective SiPMs and the light velocity inside the material. Moreover, the time at which gamma interacted with the strip can be determined as an arithmetic mean of them. Having these information, one can construct corresponding line of response and then find the position of the occured e^+e^- annihilation event [2, 19, 26].

4 Determination of the Total Body J-PET sensitivity using GATE software

One of the commonly used and accepted softwares for Monte-Carlo simulations of PET prototypes is developed by the OpenGATE Collaboration. Geant4 Application for Tomography Emission (GATE) [11, 12, 13, 14] is an advanced opensource simulation toolkit based on Geant4 software [15, 16, 17] dedicated to numerical simulations in medical imaging and radiotherapy. It allows to design and study new geometries and simulate data for image reconstruction. The GATE software was used to simulate the Total Body PET systems proposed by the Jagiellonian PET Collaboration.

In total, two groups of three geometries were simulated. The first group of tomographs is based on a plastic scintillator strip with dimensions of $6 \times 30 \times 2000$ mm. 16 of such strips arranged in a side by side manner with a 0.5 mm gap in between constitutes a panel. The only difference between the three geometries within the first group lies in the panel arrangement inside the superior construction – module. First type of module is composed of two panels situated one over another, where between them there is an additional layer of wavelength shifters (WLS) (see Figure 7.A). This 3 mm thick layer consists of WLS strips arranged perpendicularly to the scintillator strips [40]. Its main purpose is to improve the reconstruction of the annihilation photon's interaction point, by improving its axial spatial resolution. Second variant has similar structure, but with an additional layer of WLS-s and one more panel (see Figure 7.B). The third and last type consists of four modules however, in that case there are also only two WLS layers, one between 1st and 2nd panel and second between 3rd and 4th panel (see Figure 7.C). Such arrangement is caused due to the fact that a single panel only needs a one-way WLS reading in order to limit the range of hit's axial coordinate. Finally, in each case a ring of 24 modules with inner radius equal to 39.3 cm forms the cylindrical tomograph geometry. The second group of the Total Body J-PET variants consists of three systems of exactly same construction, with the only exception in the plastic scintillator dimensions, which is changed to $6 \times 30 \times 2500$ mm.

In order to determine the sensitivity (see Chapter 2.2) of the proposed tomographs, two kinds of simulations were performed for each of them: one with a line source of back-to-back 511 keV photons and one with the same line source covered with a cylindrical phantom filled with water. In both cases, the 1 MBq source was situated in the center of the scanner and its length was set to 250 cm. This number corresponds to filling of the whole AFOV of the longest proposed Total Body J-PET scanner and allows for calculation of sensitivity of every possible to detect axial source placing. The centrally located water filled cylindrical phantom with 10 cm radius was used in order to mimic the patient body. The length of the phantom was set to 183 cm, which is the average man height in the tallest country in the world [1].

The interaction of 511 keV gammas with plastic scintillators takes place mainly via Compton scattering. Because of that, the usually used in case of inorganic crystal scintillators energy window criterion was exchanged for energy threshold and set to 200 keV [27]. Moreover, the energy resolution was introduced into the simulation. The energy blurring process in GATE software simulates Gaussian blurring of the energy spectrum of registered hits by introducing a resolution R_0 (FWHM), at a given energy E_0 and then following the inverse square law [41]:

$$R = R_0 \frac{\sqrt{E_0}}{\sqrt{E}} \ , \tag{5}$$

where E denotes measured hit energy and R – the corresponding resolution. In this simulations the resolution R_0 was set to 0.18 at the energy $E_0 = 511$ keV [26]. Finally, the

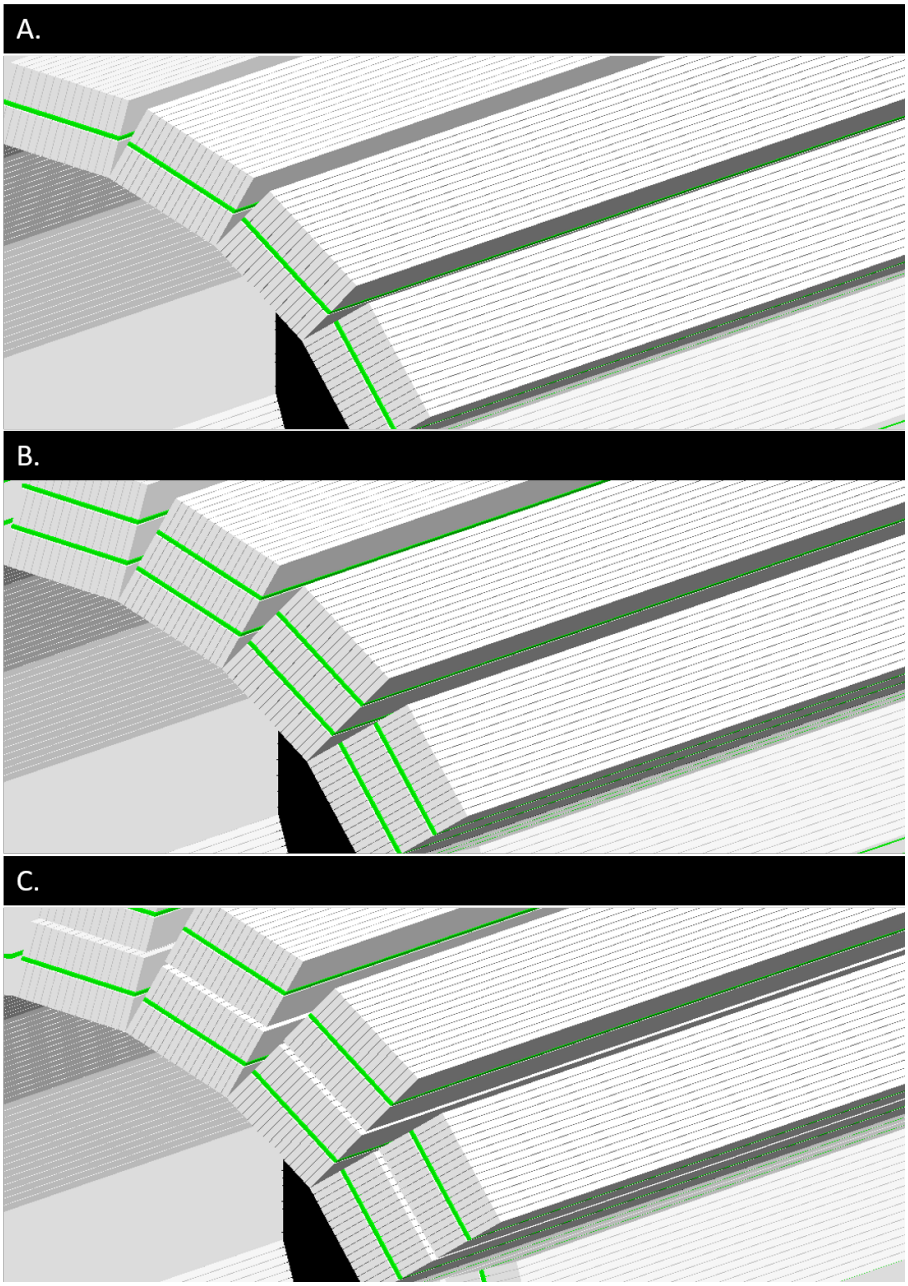

Figure 7: Schematic view of three different module compositions utilized in the proposed TB J-PET systems and simulated with the GATE software. From the top: A. 2 panels with 1 WLS layer; B. 3 panels with 2 WLS layers; C. 4 panels with 2 WLS layers.

time window used for pairing of hits into coincidences was set to 5 ns.

The total sensitivities of each TB J-PET geometry calculated according to Equation 1 (or Equation 3 in case of simulation with the phantom) are presented in Table 1. The corresponding sensitivity profiles are shown in Figures 8a and 8b, for simulation without and with phantom respectively (see Equations 2 and 4). Moreover, an additional numerical result – sensitivity at center – is presented in Table 1. The sensitivity at center (S_{center}) is equal to the sensitivity (S_i or S_i^{ph}) of the central slice (at 0 cm) and represents maximal possible efficiency of photon registration. Each of uncertainties presented in Tables 1 and 2 are statistical errors estimated as a square root of either total number of simulated

registered events (in case of total sensitivities) or number of counts in the central bin (in case of sensitivity at center).

Introduced in the Total Body PET systems significantly extended FOV contributes positively to the sensitivity of the tomograph due to possibility of detection of large angle variety of lines of responses. However, high attenuation, increase in phantom scatters and parallax error of the most oblique LORs have an unfavorable influence on another important PET characteristic – the spatial resolution. Because of that, in this type of scanners the acceptance angle criterion is being widely used as an attempt to optimize PET performance. Acceptance angle is a maximum azimuthal angle for which the line of responses are still taken into image reconstruction. Therefore it is important to check the sensitivity after this necessary cut [42].

In case of the Total Body J-PET systems build from long plastic scintillator strips, this criterion was recently estimated to 45 degree angle [42]. Recalculated numerical results, as well as sensitivity profiles for each of six TB J-PET variants are presented in Table 2 and Figures 9a and 9b.

Simulations of the Total Body J-PET scanners using GATE software indicate that, as expected, there is a visible improvement in the sensitivity with extension of the field of view, as well as with introduction of more complex module structure (addition of more panels). Based on the sensitivity profile presented in Figure 8b, 200 cm axial FOV creates an almost uniform sensitivity along the central region of the phantom, which mimics human body. Moreover, application of 250 cm long field of view not only expands the uniform region to the whole length of phantom but also creates an increase at it both ends. This increase is caused by the almost attenuation-free course of one of the back-to-back 511 keV photons emitted at the edge of phantom. Such behavior was not visible for the shorter tomograph, because there, the length form the edge of phantom to the end of tomograph was equal to only 8.5 cm, while for 250 cm of AFOV it is 33.5 cm.

The use of the 45° acceptance angle cut is creating or extending the uniform sensitivity region in case of simulations with and without the phantom (see Figures 9a and 9b). However, because it introduces a trade-off between sensitivity and spatial resolution, it gives a ∼23% (∼29%) reduction in the total sensitivity and ∼40% (∼44%) in the sensitivity at center in case of simulation with only linear source for 200 cm (250 cm) of AFOV. Nevertheless, when it comes to the more realistic simulation with phantom, the percentage reduction drop to ∼11% (∼25%) and ∼18% (∼18%) for total sensitivity and sensitivity at center, respectively and for 200 cm (250 cm) long tomograph.

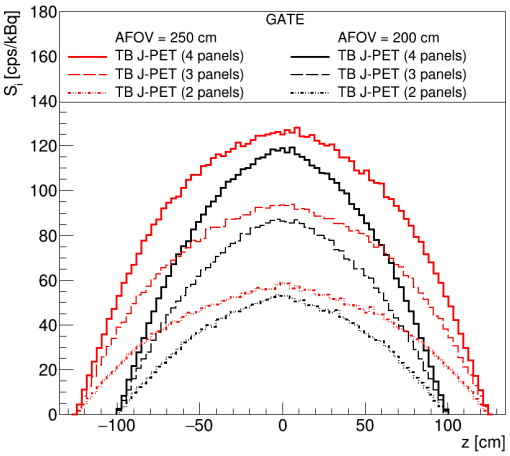

(a) Sensitivity profiles based on the simulation with a linear source.

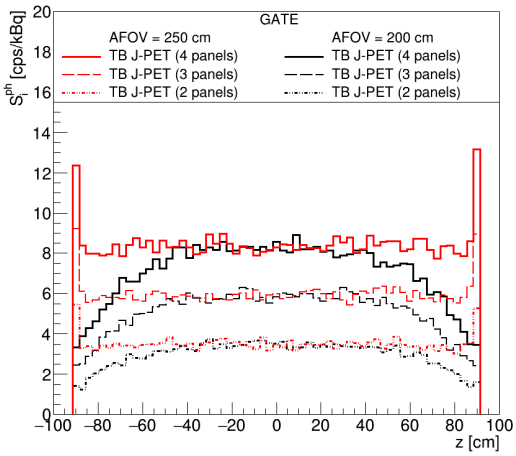

(b) Sensitivity profiles based on the simulation with 183 cm long phantom.

Figure 8: Sensitivity profiles of proposed Total Body J-PET tomographs.

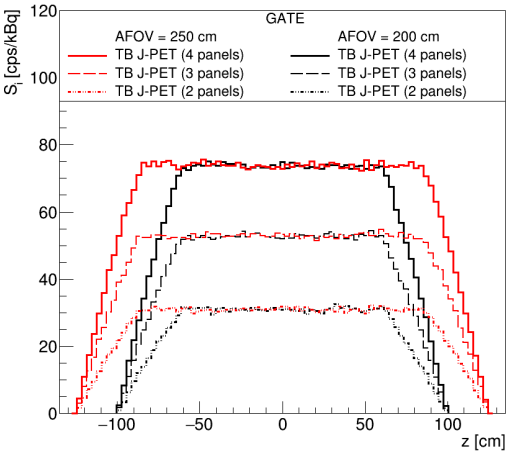

(a) Sensitivity profiles based on the simulation with a linear source.

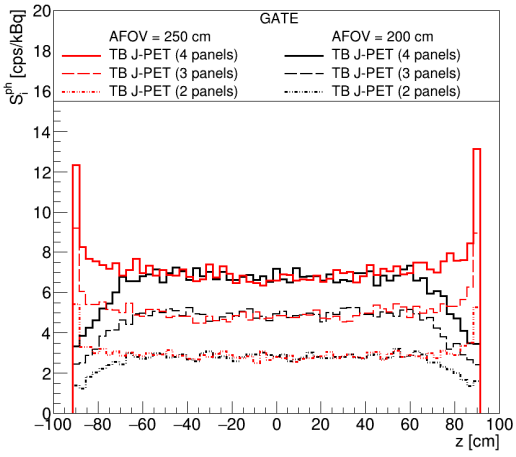

(b) Sensitivity profiles based on the simulation with 183 cm long phantom.

Figure 9: Sensitivity profiles of proposed Total Body J-PET tomographs after the acceptance angle cut on 45°.

Table 1: Total sensitivity and sensitivity at center of Total Body systems proposed by the J-PET Collaboration.

TB J-PET geometry		Simulation with source		Simulation with source & phantom	
Module	AFOV [cm]	S_{tot} [cps/kBq]	S_{center} [cps/kBq]	S_{tot}^{ph} [cps/kBq]	S_{center} [cps/kBq]
2 panels	200	26.21(05)	52.95(67)	2.97(02)	3.52(17)
3 panels	200	44.07(07)	86.13(86)	5.05(03)	5.83(22)
4 panels	200	60.92(08)	119.0(1.0)	7.09(03)	8.57(27)
2 panels	250	37.14(06)	58.91(71)	3.51(02)	3.44(17)
3 panels	250	62.12(08)	93.48(89)	5.99(03)	5.98(23)
4 panels	250	85.47(09)	125.2(1.0)	8.47(03)	8.29(27)

Table 2: Total sensitivity and sensitivity at center of Total Body systems proposed by the J-PET Collaboration after the acceptance angle cut on 45°.

TB J-PET geometry		Simulation with source		Simulation with source & phantom	
Module	AFOV [cm]	S_{tot} [cps/kBq]	S_{center} [cps/kBq]	S_{tot}^{ph} [cps/kBq]	S_{center} [cps/kBq]
2 panels	200	19.88(05)	30.95(51)	2.64(02)	2.84(16)
3 panels	200	33.84(06)	52.03(67)	4.53(03)	4.94(20)
4 panels	200	47.42(07)	74.93(80)	6.31(03)	7.19(25)
2 panels	250	25.94(05)	31.77(52)	2.99(02)	2.80(15)
3 panels	250	44.32(07)	53.20(67)	5.14(03)	4.85(20)
4 panels	250	61.90(08)	72.77(79)	7.25(03)	6.60(24)

5 Toy Monte-Carlo model for sensitivity studies

Studies of the PET scanners using GATE software are certainly the most accurate. They contain the full information about all interactions and events. Their application goes beyond sensitivity analysis and allows for image reconstruction. However, in order to check any of the parameters of the prototype tomograph, like studied in this thesis sensitivity, one has to carry out a full, usually time-consuming simulation and needs a specific set of skills since performing of such simulation is not a simple task. Moreover, any change in the geometry concerning for example thickness of the scintillator material, axial FOV or radius of the tomograph requires rewriting and rerunning simulations. If one is interested in study of the dependence of sensitivity on the detector material and geometry dimensions or even just simply wants to check new geometry idea in context of sensitivity and compare it to other possibilities, this approach for computer simulations is unnecessarily long and not all of the long-collected data is needed.

5.1 Analytical approach

Instead of the full Monte-Carlo approach, one can perform simplified analytical simulations of the sensitivity using the following formula [7, 43]:

$$S = \int_{z=0}^{z=AFOV/2} dz \left[\int_{\theta_{min}(z)}^{\theta_{max}(z)} (\epsilon_{det}(\theta) \cdot Att(\theta))^2 \cdot \sin\theta \; d\theta \right] \cdot \epsilon_{sel}^2 / L_{source} \quad , \tag{6}$$

assuming the use of:

- axially symmetric cylindrical geometry of the PET scanner,
- uniform distribution of activity in the centrally located source,
- cylindrical, centrally located phantom.

In the above formula θ denotes the polar angle between the emitted from the source photon's direction of flight and the main axis of the tomograph and L_{source} is the length of the source. The $\epsilon_{det}(\theta)$ term denotes detection efficiency as a function of the θ angle calculated as [7, 43]:

$$\epsilon_{det}(\theta) = 1 - e^{-\mu \cdot d / \sin\theta} \quad , \tag{7}$$

where μ is the linear attenuation coefficient for 511 keV photon for scintillator material and d is its radial thickness. The $Att(\theta)$ indicates fraction of annihilation photons which does not interact with the phantom. According to the initial assumption about the phantom, this term can be estimated as [7, 43]:

$$Att(\theta) = e^{-\mu_{phantom} \cdot R_{phantom} / \sin\theta} \quad , \tag{8}$$

where $\mu_{phantom}$ is the linear attenuation coefficient for 511 keV photon for the cylindrical phantom material with radius $R_{phantom}$. The angular range of the inner integral determines the angular acceptance (solid angle) of the tomograph for the back-to-back gamma emission from the annihilation inside the source, at the z point along the central axis. Finally, the ϵ_{sel} stands for selection efficiency of taken into image reconstruction annihilation photons. It is estimated as a fraction of the process which contributes the most to the detection. For crystal scintillators it is a fraction of the photoelectric effect, whereas for the plastic scintillators it comes from Compton effect [7, 43].

In case when the source is shorter than the AFOV, the outer integral in the formula 6 should be performed over the range from $AFOV/2 - L_{source}/2$ to $AFOV/2$ [7].

Although this method gives approximate results of sensitivity, especially gains of sensitivity between different geometries, very quickly, it has a few drawbacks:

1. The length of the phantom is unchangeable. It is by design infinite.
2. Only the intersection of photon's flight path with the face of the scintillator detectors is checked for containing inside the axial FOV. It may happen that if a photon enters the detector situated near the edges of the scanner, the z component of the detection point will be outside of the AFOV.
3. It is not valid for the, so-called, sparse geometries which have only partial coverage of the field of view with detectors.

Therefore, in this thesis a different approach to sensitivity simulation was proposed, which is an extension of the described analytical method to include and resolve mentioned problems.

5.2 Principle of operation of the proposed Toy Monte-Carlo approach

The concept of the proposed method is based on the analytical approach but uses simplified Monte-Carlo simulation for events generation in oppose to calculating the integral over possible annihilation positions. Separate generation of each event allows to track the path of flight of both photons and addresses the second and third of the previously mentioned problems. Moreover, it includes the possibility of finite-length phantoms. However, this method works only with the same assumptions about the symmetry of geometry, source and phantom as in the analytical version. Together with the knowledge of the isotropic emission of the annihilation photons, they allow to bring down a 3 dimensional problem to just 2 dimensions. Symmetry ensures that the system remains invariant with respect to rotation around the central axis of a scanner, so for each event only the z position of annihilation and the polar angle of emission θ are being simulated.

In order to run simulation, only a few parameters are needed:

- Time of simulation
- Activity of the source
- Length of the line source
- Scintillator material
- Radial thickness of the scintillator material
- Axial filed of view in case of full geometries or sensitive sections in case of sparse geometries

with an addition of:

- Phantom material
- Phantom length
- Phantom radius

in case of simulation with a phantom. A detailed step-by-step description of the principle of operation of this approach is as follows:

1. To begin with, the z coordinate of the annihilation event is simulated with the uniform probability within the setted line source. Additionally to this, cosine of angle θ is being simulated, again with the uniform probability. Because each event results in creation of back-to-back 511 keV photons, only one such angle per event is needed.

2. Secondly, the chance of interaction of each annihilation gamma with phantom material is found separately. Knowing the length and radius of the cylindrical phantom, the length D_{ph} of the photon path inside it can be determined. Then the probability of the interaction for this length is calculated as $1 - e^{-\mu_{phantom} \cdot D_{ph}}$, where $\mu_{phantom}$ is the linear attenuation coefficient for 511 keV photon in phantom material. Next, according to this probability, it is decided whether the photon interacted in the phantom. If any of the two, back-to-back photons interacted with the material, such event is discarded. This step is followed only for a simulation with a phantom.

3. In the next step the detection efficiency for each gamma is determined similarly as in formula 7. However, in order to consider possibilities of sparse geometries and introduce corrections for false detections on the sides of a tomograph, a real maximal length of the photon path inside the detector is calculated. Moreover, the exact position of interaction with detector material (hit) is also simulated. This opens a possibility for making post-simulation angle based or ring based cuts, which reflect the angular acceptance of LORs.

4. Finally, event is taken into account only if both of the registered gammas pass the selection efficiency criterion. While in the analytical approach this parameter was established as a fraction of most contributing process to the detection in scintillator material, in this method it also takes into consideration detection via multiple energy depositions inside the detector based on Compton scatter. Further description of this evaluation is provided in the Chapter 5.3.

As a result of the simulation a list of z components of annihilation and both hit positions per recorded event is obtained. This information allows for not only calculation of total sensitivity but also for creation of sensitivity profiles in dependence on angular acceptance of LORs, which was not possible in case of the analytical formula 6. However, only events resulting in the true coincidences (see Figure 2.A.) are being registered. Rejection of events in which any of the photons interacted with the phantom removes the possibility for scattered coincidences and using an event-by-event technique without time component removes random and multiple coincidences.

5.3 Study of photon registration efficiency

The principle of operation of PET tomography lies in the detection of pairs of photons originating in annihilation events by scintillator detectors. In case of inorganic scintillator materials, the detection takes place mainly via photoelectric effect in which 511 keV gamma deposits all of its energy. However, there is a considerable amount of events when photon scatters on the atoms of the medium depositing only part of the carried energy. Then, it can travel to one of the adjacent detectors and scatter once more. This procedure can repeat itself many times. Due to the fact that single scintillator detector has a small volume and any scattered photon will most probably exit its interior, in order to benefit also from such

events many tomographs work on array-based principle. Each array consists of several to several dozen detectors and during the coincidence based detection, it sums up all energies deposited within coincidence time window. If the total energy meets the requirement of energy window, the detection is being registered. In case of organic scintillator materials for which the Compton scatter is the most contributing to the detection process, it is necessary to have a large volume taken into account during registration. However, because of the much cheaper production of organic scintillators in oppose to inorganic ones, the large volume of material can be introduce as a single detector.

Presented in the Chapter 5.1 analytical method of sensitivity calculation, takes into consideration as a selection efficiency only the process which contributes the most to the detection. In order to correct this parameter for also multiple scattering events, a simplified GATE simulation was performed for each of 2 meter long TB J-PET geometries. For simplicity, only one module of each of them was used during simulation together, with the 250 cm long line source of 1 MBq activity. The distance between them was set to 39.3 cm, which corresponds to the TB J-PET radius. Deposited energy underwent smearing procedure as described in Chapter 4. The corrected selection efficiency ϵ_{sel}^{corr} was determined as the fraction of photons which deposited enough energy to pass the 200 keV energy threshold to the total amount of photons interacting with the scintillators. As both of these values have corresponding statistical errors estimated as their square roots, the ϵ_{sel}^{corr} statistical uncertainty was calculated with the propagation of uncertainty technique. Resulting factors were equal to 0.455(04), 0.467(03), 0.474(03) for modules consisting of 2, 3 and 4 panels respectively.

Furthermore, the dependence of selection efficiency on the scintillator length was inspected in the similar manner for 2 panels module and presented in Figure 10. The obtained result shows in good approximation that there is no relation between corrected selection efficiency and AFOV, ϵ_{sel}^{corr} is constant. Due to that fact, the same ϵ_{sel}^{corr} values were used also for second group of studied tomographs (with 250 cm long AFOV).

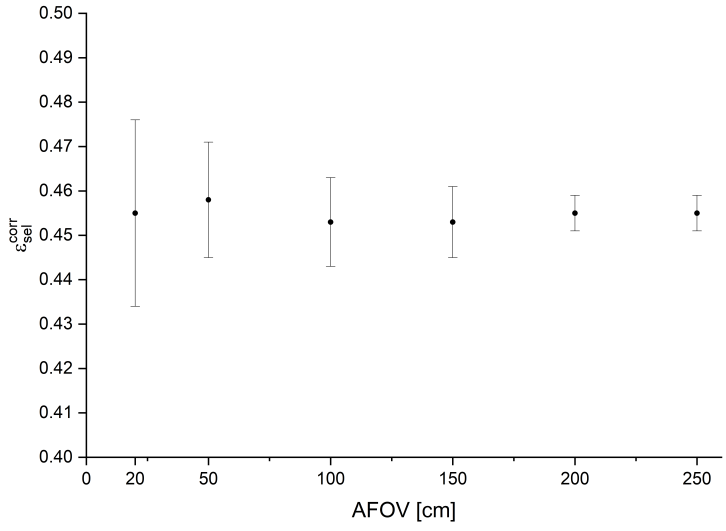

Figure 10: Dependence of corrected selection efficiency factor on plastic scintillator strip length (AFOV).

5.4 Validation of the proposed model

To validate the Toy Monte-Carlo approach simulations for each of the investigated Total Body J-PET systems presented in Chapter 4 were performed. Similarly as in case of using GATE software, two types of simulations with identical parameters were conducted: with and without the phantom. The values of linear attenuation coefficients for 511 keV photons (as described in Chapter 5.1) were assumed to be $\mu \equiv \mu_{Plastic} = 0.096$ cm^{-1} and $\mu_{phantom} \equiv \mu_{Water} = 0.096$ cm^{-1}. The quoted values of attenuation coefficients were extracted from the National Institute of Standards and Technology's data base [44]. The study of corrected selection efficiency for plastic scintillators was presented in the Chapter 5.3. Finally, the radial thickness of the scintillator material was assumed to 6, 9 and 12 cm for modules consisting of 2, 3 and 4 panels respectively. The contribution of the WLS layers and the air-filled gaps between elements was neglected, as their are not sensitive parts to the main hit registration. A comparison between the results obtained with both methods was done for sensitivity profiles (see Figures 11 and 12) and numerical results (see Tables 11 and 12).

In case of results coming from the GATE simulation the presented uncertainties are statistical errors estimated as square root of number of counts (see Chapter 4). However, in case of Toy Monte-Carlo approach, apart from the similar statistical uncertainty there is also a systematic uncertainty. It is originating from the corrected selection efficiency, as it is a parameter burdened with error, that affects the Monte Carlo generation of events used in the analysis. Due to the fact that the effects of this uncertainty cannot be followed through combination of errors algebra, the Barlow method was used to evaluate the systematic uncertainty [45]. Assuming that the final result R depends on the parameter a, which is estimated to a_0 with uncertainty σ_a, one can repeat the simulation for $a = a_0 - \sigma_a \Rightarrow R_-$ and $a = a_0 + \sigma_a \Rightarrow R_+$. Based on the obtained results (R_-, R and R_+) one can calculate $R' = \frac{dR}{da}$. The final systematic error to the result R is then assumed as $\sigma_a R'$ [45]. Henceforth, the numerical results coming from the Toy Monte-Carlo and presented in every table will possess both statistical uncertainty (before $\pm$ sign) and systematic uncertainty (after $\pm$ sign).

In order to present the post-simulation analysis capability of the Toy Monte-Carlo model, a comparison between the results after the acceptance angle cut was carried out and presented in Figures 13 & 14 and in Tables 13 & 14.

Performed comparisons show, that the introduced simplified model reproduces the results from the standard computer simulations with GATE software very well, especially in case of simulating only radioactive source. For simulations of 2.5 meter long J-PET geometry with the phantom it recreates the sensitivity gains on its sides. This behavior confirms that the infinite phantom problem existing in the analytical approach is here resolved. Moreover, this method enables correct angular acceptance cuts with a small overestimation in case of simulation without phantom.

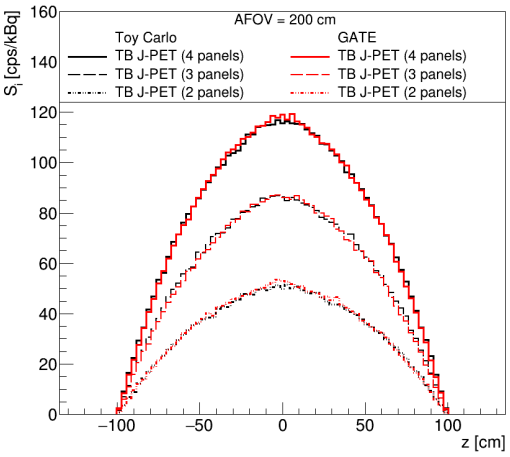

(a) Comparison of sensitivity profiles based on the simulation with a linear source for 2 meter long TB J-PET geometries.

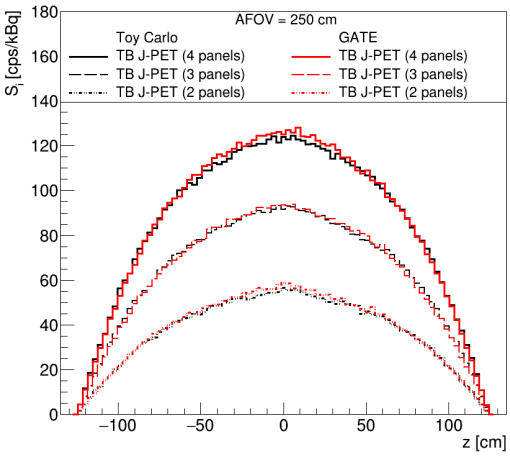

(b) Comparison of sensitivity profiles based on the simulation with a linear source for 2.5 meter long TB J-PET geometries.

Figure 11: Comparison of sensitivity profiles based on the simulation with a linear source for the proposed Total Body J-PET tomographs.

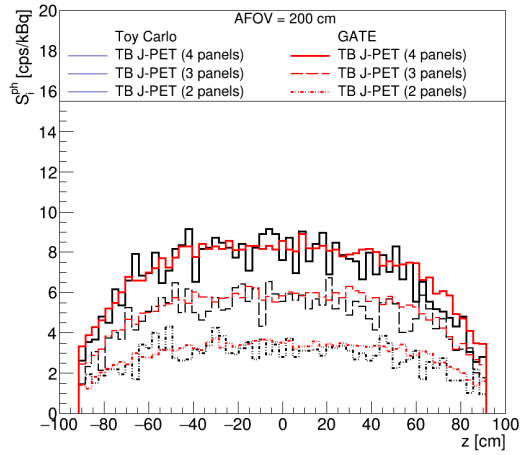

(a) Comparison of sensitivity profiles based on the simulation with 183 cm long phantom for 2 meter long TB J-PET geometries.

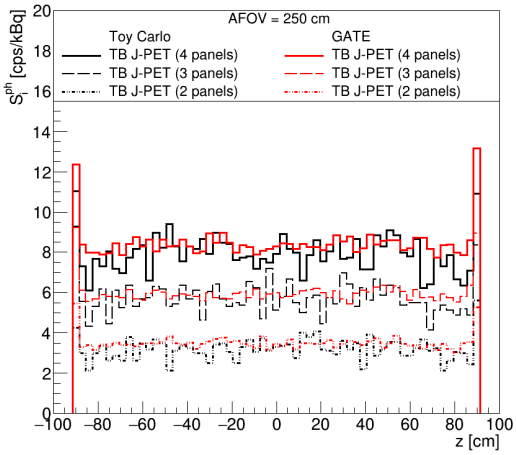

(b) Comparison of sensitivity profiles based on the simulation with 183 cm long phantom for 2.5 meter long TB J-PET geometries.

Figure 12: Comparison of sensitivity profiles based on the simulation with 183 cm long phantom for the proposed Total Body J-PET tomographs.

Table 3: Total sensitivity and sensitivity at center of Total Body J-PET scanners simulated with Toy Monte-Carlo and GATE software and based on the simulation with a linear source.

TB J-PET geometry		GATE		Toy Monte-Carlo	
Module	AFOV [cm]	S_{tot} [cps/kBq]	S_{center} [cps/kBq]	S_{tot} [cps/kBq]	S_{center} [cps/kBq]
2 panels	200	26.21(05)	52.95(67)	25.92(05±04)	49.94(65±37)
3 panels	200	44.07(07)	86.13(86)	44.60(07±06)	86.27(86±83)
4 panels	200	60.92(08)	119.0(1.0)	60.91(08±07)	115.6(1.0±1.6)
2 panels	250	37.14(06)	58.91(71)	36.46(06±07)	56.6(0.7±1.6)
3 panels	250	62.12(08)	93.48(89)	62.21(08±08)	91.50(88±65)
4 panels	250	85.47(09)	125.2(1.0)	84.7(0.9±1.1)	124.1(1.0±1.1)

Table 4: Total sensitivity and sensitivity at center of Total Body J-PET scanners simulated with Toy Monte-Carlo and GATE software and based on the simulation with a phantom.

TB J-PET geometry		GATE		Toy Monte-Carlo	
Module	AFOV [cm]	S^{ph}_{tot} [cps/kBq]	S_{center} [cps/kBq]	S^{ph}_{tot} [cps/kBq]	S_{center} [cps/kBq]
2 panels	200	2.97(02)	3.52(17)	2.77(06±08)	3.11(51±30)
3 panels	200	5.05(03)	5.83(22)	4.81(08±08)	5.86(71±50)
4 panels	200	7.09(03)	8.57(27)	6.85(10±07)	9.0(0.9±1.0)
2 panels	250	3.51(02)	3.44(17)	3.19(07±08)	3.48(54±88)
3 panels	250	5.99(03)	5.98(23)	5.74(09±06)	5.31(67±77)
4 panels	250	8.47(03)	8.29(27)	7.94(11±45)	8.66(86±90)

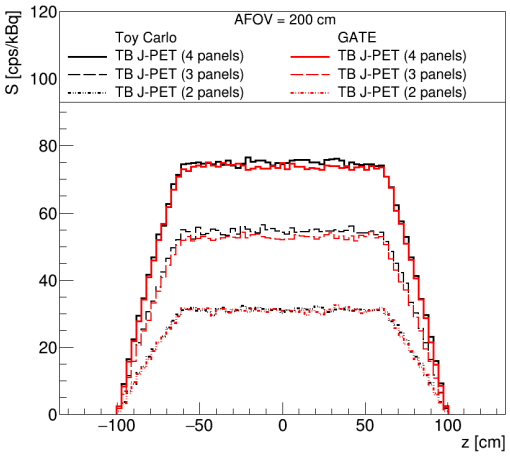

(a) Comparison of sensitivity profiles based on the simulation with a linear source for 2 meter long TB J-PET geometries.

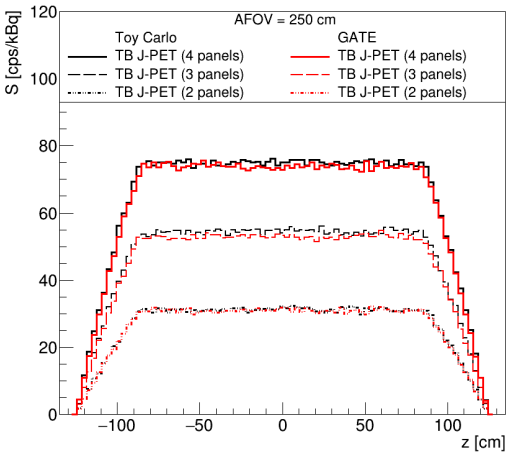

(b) Comparison of sensitivity profiles based on the simulation with a linear source for 2.5 meter long TB J-PET geometries.

Figure 13: Comparison of sensitivity profiles based on the simulation with a linear source for the proposed Total Body J-PET tomographs after the acceptance cut on 45°.

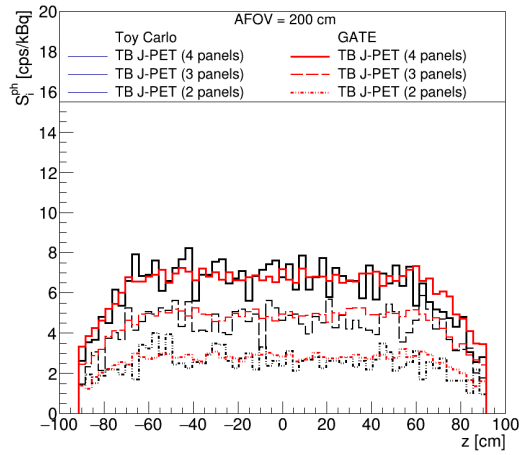

(a) Comparison of sensitivity profiles based on the simulation with 183 cm long phantom for 2 meter long TB J-PET geometries.

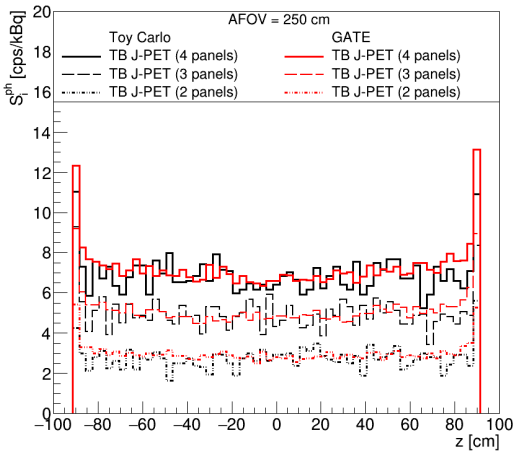

(b) Comparison of sensitivity profiles based on the simulation with 183 cm long phantom for 2.5 meter long TB J-PET geometries.

Figure 14: Comparison of sensitivity profiles based on the simulation with 183 cm long phantom for the proposed Total Body J-PET tomographs after the acceptance cut on 45°.

Table 5: Total sensitivity and sensitivity at center of Total Body J-PET scanners simulated with Toy Monte-Carlo and GATE software and based on the simulation with a linear source. Moreover, the angular acceptance cut on 45° was used.

TB J-PET geometry		GATE		Toy Monte-Carlo	
Module	AFOV [cm]	S_{tot} [cps/kBq]	S_{center} [cps/kBq]	S_{tot} [cps/kBq]	S_{center} [cps/kBq]
2 panels	200	19.88(05)	30.95(51)	20.08(05±05)	30.23(51±48)
3 panels	200	33.84(06)	52.03(67)	35.08(06±05)	54.1(0.7±1.0)
4 panels	200	47.42(07)	74.93(80)	48.26(07±06)	74.42(80±43)
2 panels	250	25.94(05)	31.77(52)	26.24(05±08)	32.27(52±65)
3 panels	250	44.32(07)	53.20(67)	45.69(07±06)	54.03(68±80)
4 panels	250	61.90(08)	72.77(79)	62.96(08±05)	75.1(0.8±1.1)

Table 6: Total sensitivity and sensitivity at center of Total Body J-PET scanners simulated with Toy Monte-Carlo and GATE software and based on the simulation with a phantom. Moreover, the angular acceptance cut on 45° was used.

TB J-PET geometry		GATE		Toy Monte-Carlo	
Module	AFOV [cm]	S^{ph}_{tot} [cps/kBq]	S_{center} [cps/kBq]	S^{ph}_{tot} [cps/kBq]	S_{center} [cps/kBq]
2 panels	200	2.64(02)	2.84(16)	2.48(06±04)	2.62(47±25)
3 panels	200	4.53(03)	4.94(20)	4.30(08±09)	4.45(62±47)
4 panels	200	6.31(03)	7.19(25)	6.18(09±08)	7.87(82±51)
2 panels	250	2.99(02)	2.80(15)	2.76(06±08)	2.87(49±63)
3 panels	250	5.14(03)	4.85(20)	5.00(08±07)	4.39(61±45)
4 panels	250	7.25(03)	6.60(24)	6.90(10±11)	7.56(80±70)

Furthermore, to validate the investigated approach also for tomographs build with inorganic crystal scintillators, two additional PET systems were chosen: uEXPLORER as another Total Body PET and Biograph Vision from the Siemens Healthineers [46] as a conventional, short AFOV tomograph. At the same time, these scanners show a possibility of introducing sparse-like geometries into proposed model, as both of them consists of detector rings separated by small gaps, not continuous scintillators.

uEXPLORER

The Total Body uEXPLORER PET tomograph consists of 8 detector rings of 78.6 cm inner diameter, which provide the 194.8 cm axial field of view. Each 24.02 cm wide ring is composed of 24 panels, while every panel is a composition of 70 arrays of 42 LYSO crystal scintillators with dimensions of $2.76 \times 2.76 \times 18.1$ mm^3 [47]. In order to make a comparison, simulations with 2.5 meter long linear source of 1 MBq activity using both GATE and Toy Monte-Carlo model were performed. The energy window for hit registration was set to 430-645 keV [47]. The energy resolution R_0 was assumed as 0.117 at the energy $E_0 - 511$ keV [7]. The time window for coincidence based registration was set to 5 ns. Moreover, similarly as in case of the Total Body J-PET tomographs, the corrected selection efficiency, while taking into account array-based principle of detection (see Chapter 5.3) was estimated. For simplicity, dedicated GATE simulation consisted of only one array of scintillators and a 10 cm long linear source with 1 MBq activity. The resulting corrected selection efficiency was equal to 0.678(04). The linear attenuation coefficient value for 511 keV photons was assumed to be $\mu \equiv \mu_{LYSO} = 0.82$ cm^{-1} [44].

The final comparison between both simulation is presented in Figure 15a and Table 7. Additionally, an angular acceptance criterion was introduced. However, due to the fact that uEXPLORER utilizes separate detector rings, instead of performing angle based cut, one has to use a ring based cut. Such criterion confines the hit pairing to the maximum of few rings difference, which in case of this scanner was set to 4 [47].

Biograph Vision

Till now every inspected PET tomograph was representing a Total Body category. To include into the validation also a conventional system with short axial field of view, the Biograph Vision scanner from the Siemens Healthineers was chosen. It consists of eight 3.2 cm wide rings constructed of 38 arrays of 10×20 LSO crystals. Each crystal has a dimension of $3.2 \times 3.2 \times 20$ mm^3. In total, the system provides 26.3 cm of AFOV with 82 cm inner diameter [48]. In order to perform a comparison of sensitivity calculation methods, the same simulation as in case of uEXPLORER was done. The assumed values of parameters needed for coincidence creation were: 435-650 keV energy window [48], 4.73 ns time window [48] and 0.1 energy resolution at 511 keV energy [49]. Next, the corrected selection efficiency was estimated by taking only one array of crystals (same as with uEXPLORER) to 0.784(09). The last required parameter – the linear attenuation coefficient for 511 keV photons in LSO material was assumed to $\mu \equiv \mu_{LSO} = 0.87$ cm^{-1} [44]. Figure 15b shows the sensitivity profile of Biograph Vision obtained with GATE and Toy Monte-Carlo. The comparison of numerical results (total sensitivity and sensitivity at center) is presented in Table 7.

The comparisons performed for additional PET scanners validate the investigated model for standard tomographs build from inorganic crystal scintillators. They show the possibility of applying not only angle based acceptance cuts but also ring based cuts. Finally, they also present the ability of simulating non-continuous configurations with gaps between detectors.

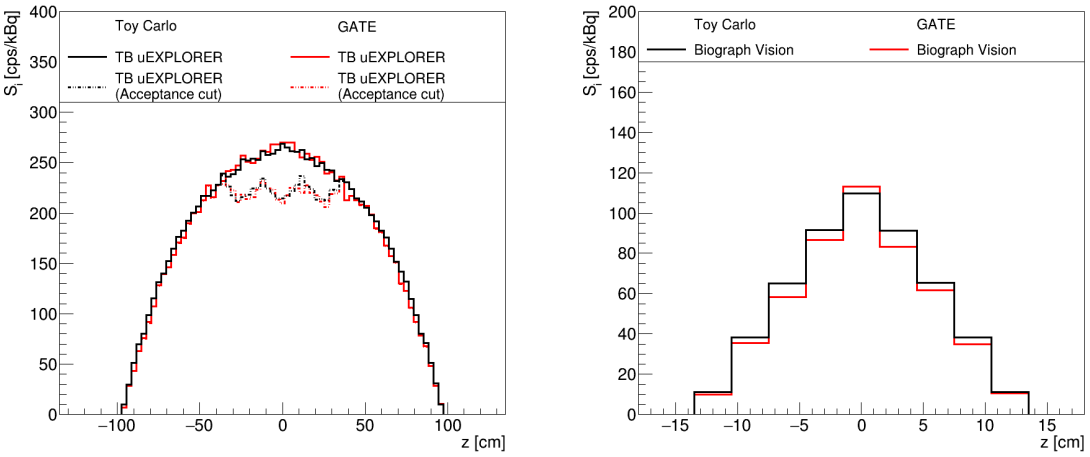

(a) Comparison for the Total Body uEXPLORER system.

(b) Comparison for the Biograph Vision system.

Figure 15: Comparison of sensitivity profiles based on the simulation with a linear source.

Table 7: Total sensitivity and sensitivity at center of uEXPLORER and Biograph Vision tomographs simulated with Toy Monte-Carlo and GATE software and based on the simulation with a linear source.

	GATE		Toy Monte-Carlo	
	S_{tot} [cps/kBq]	S_{center} [cps/kBq]	S_{tot} [cps/kBq]	S_{center} [cps/kBq]
uEXPLORER	140.20(37)	269.6(4.8)	141.7(0.1±1.8)	268.4(1.5±2.6)
uEXPLORER (Acceptance cut)	130.39(36)	209.5(4.2)	133.2(0.1±1.7)	214.6(1.4±1.8)
Biograph Vision	5.81(08)	113.2(3.1)	6.14(08±02)	109.9(3.1±3.5)

6 Sensitivity of the Total Body J-PET tomographs with the Toy Monte-Carlo model

Investigated in this work Total Body tomographs made with J-PET technology can be divided in either two or three groups, according to their axial field of view or module composition (see Chapter 4). For each of the six TB J-PET variants the sensitivity profiles, as well as the numerical total sensitivities and sensitivities at center were determined using the introduced Toy Monte-Carlo model. During the calculations two type of simulations were taken into account:

1. Idealized simulation of back-to-back 511 keV photon source for estimation of NEMA alike parameters,

2. Simulation of back-to-back source situated along the center of the water filled phantom, which mimics human body.

The results of these studies were already presented in the Chapter 5.4 during the comparison tests carried out in order to validate the simplified Monte-Carlo model. The plot summarizing all of the obtained sensitivity profiles is shown in Figure 16a and 16b, for 1st and 2nd simulation type respectively. Moreover, the influence of the angular acceptance criterion introduced as a 45° cut on the oblique lines of responses was investigated and the summary of resulting sensitivity profiles is presented in Figure 17.

Similarly as in case of determination of sensitivity with the GATE software, there is a visible increase in sensitivity on both ends of the 183 cm long phantom for 2.5 meter TB J-PET scanners. It is caused by the almost attenuation-free photons emitted at the phantom edges. The almost uniform sensitivity along the phantom creates a unique possibility for high-quality simultaneous imaging of the whole patient body. While the introduction of requisite acceptance cut has a huge influence on the sensitivity in case of 1st type of simulations, its impact significantly drops for the more realistic, 2nd type simulations (see Chapter 4 as the results from GATE simulation are equivalent to the ones from the Toy Monte-Carlo). All of the results concerning total sensitivities and sensitivities at center can be found within Tables 3, 4, 5 and 6.

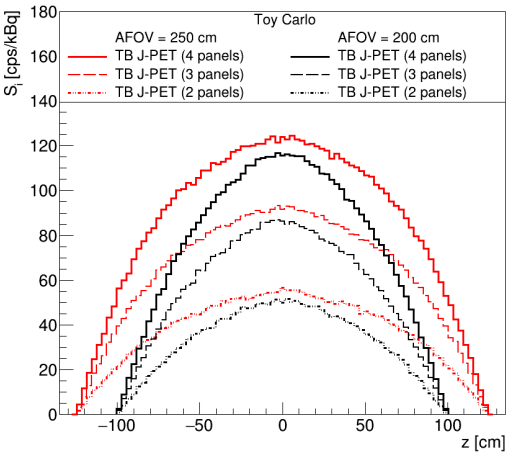

(a) Sensitivity profiles based on the simulation with a linear source.

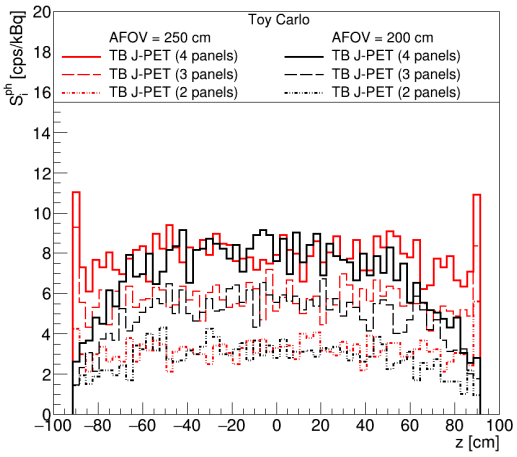

(b) Sensitivity profiles based on the simulation with 183 cm long phantom.

Figure 16: Sensitivity profiles of proposed Total Body J-PET tomographs based on the Toy Monte-Carlo model.

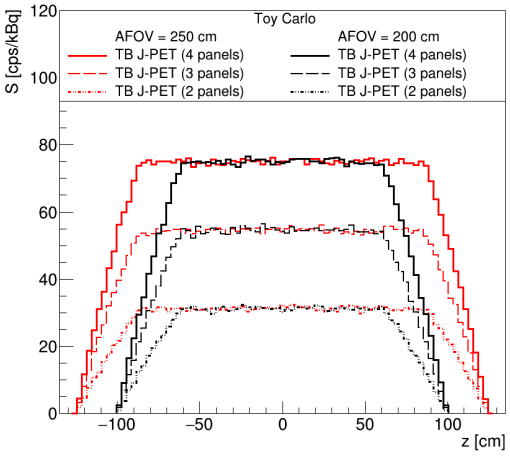

(a) Sensitivity profiles based on the simulation with a linear source.

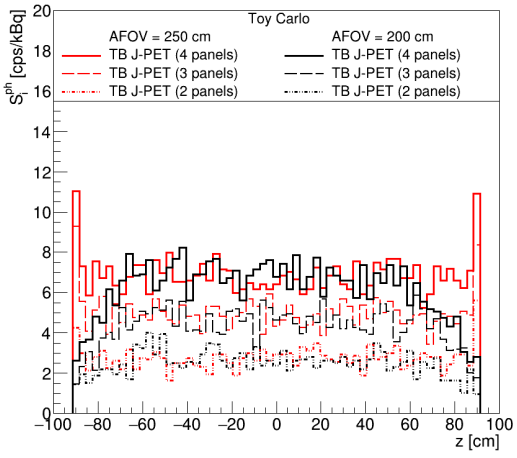

(b) Sensitivity profiles based on the simulation with 183 cm long phantom.

Figure 17: Sensitivity profiles of proposed Total Body J-PET tomographs after the acceptance angle cut on 45° and based on the Toy Monte-Carlo model.

6.1 Dependence of the sensitivity on the axial field of view

Extending of the axial field of view of PET systems causes greater detector coverage over the human body. This directly translates into increased sensitivity to the detection of any type of coincidences, including the true coincidences. However, this relation cannot be linear not only due to the growing attenuation probability inside the patient body, but also because the extension takes place in the longitudinal coordinate of the tomograph cylindrical geometry. Such expansion doesn't translate one-to-one to the solid angle coverage with detectors, while the emission of crucial back-to-back photons is isotropic. Therefore, the dependence of investigated numerical sensitivities on the axial field of view of J-PET geometries constructed with each of three introduced module types was examined. Figure 18 shows the results obtained from the idealized simulation (1st type), calculated following the NEMA procedure (Equation 1 and 2). Additionally, the influence of 45° acceptance cut was also investigated. Nonetheless its applicability starts for the AFOV longer than 78.6 cm (when the maximal possible slope of the LOR is equal 45°), and its value should be studied in more detail for each length (as in [42]) and may be subject to changes. The acquired relations are presented in Figure 19. All of the presented uncertainties take into account only statistical errors and are calculated as the square root of the total number of counts (for S_{tot}) or of the number within the central bin (for S_{center}).

The obtained results of dependence of total sensitivity, as the most NEMA-like parameter, show a slightly accelerating growing trend up to the axial field of view of around 250 cm (see Figure 18a). For AFOVs longer than 250 cm a slow decline in the overall increase in the total sensitivity begins. Such limit value is expected, since it corresponds to the length of the utilized in the simulation radioactive source. Extending the FOV of the PET tomograph as far as the possible radiation origin is not only enlarging the geometrical acceptance for already covered part of the source but also enables detection of its more and more marginal sections. Going further than source length leaves only enhancement in the geometrical acceptance, which becomes less and less significant due to the not linear relation between expansion in cylindrical coordinate system (tomograph geometry) and in spherical coordinate system (radiation emission geometry). This tendency is clearly visible while considering only the sensitivity at center (see Figure 18b). This parameter can be interpreted as the result for the point-like source situated in the axial and radial center of the PET scanner. Initially rapid growth decreases already around $\sim$ 100 cm, and above $\sim$ 200 cm it is almost negligible. Described behaviour is even more apparent, when one introduces an imperative angular acceptance criterion. As shown in Figure 19b after crossing the axial field of view's length equal to the acceptance criterion (in this case the 45° cut corresponds to the AFOV $\equiv$ tomograph radius = 78.6 cm) there are no more changes in the S_{center} value. Moreover, previous non-linear relation between total sensitivity and AFOV in the range up to source length became almost linear (see Figure 19a), as the new, extended part of the tomograph do not contribute to the registration of radiation originating from the innermost parts of the source.

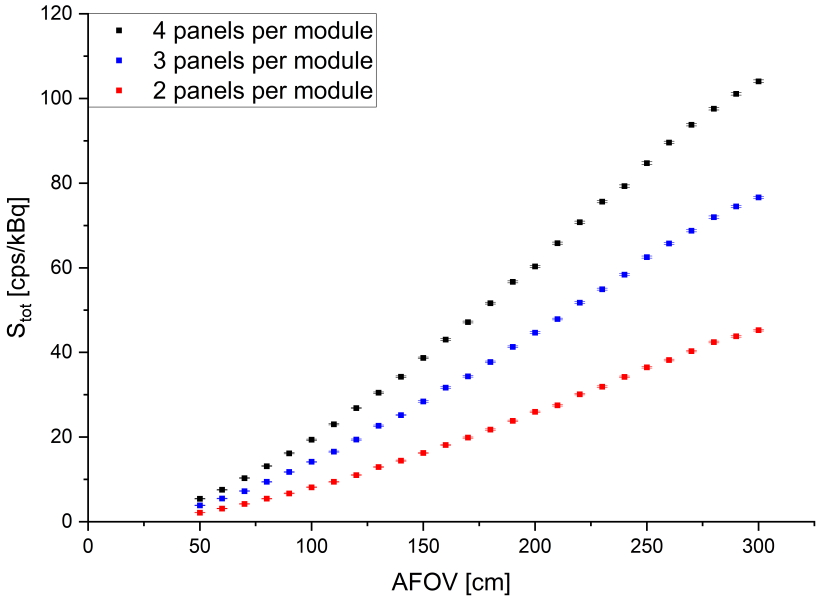

(a) Dependence of total sensitivity on AFOV.

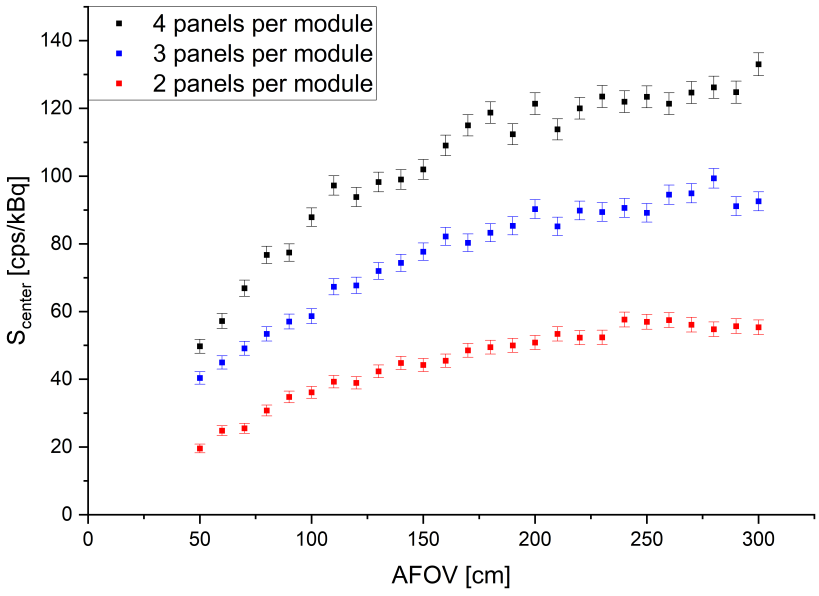

(b) Dependence of sensitivity at center on AFOV.

Figure 18: The dependence of sensitivity on the axial field of view of tomographs created with the introduced J-PET technology.

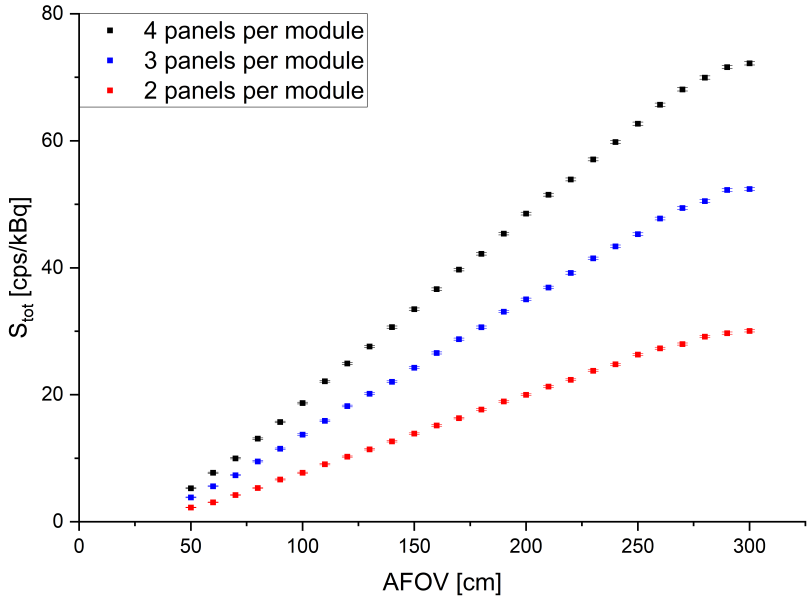

(a) Dependence of total sensitivity on AFOV.

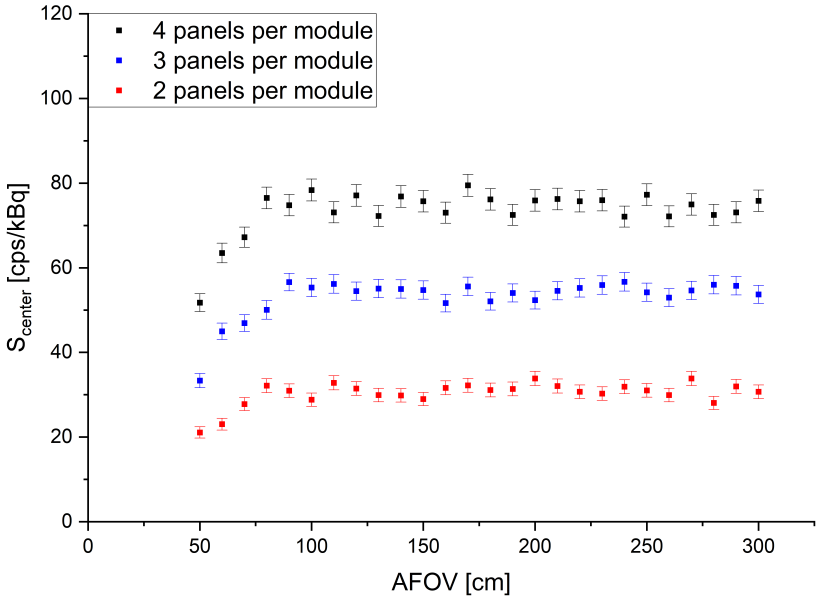

(b) Dependence of sensitivity at center on AFOV.

Figure 19: The dependence of sensitivity on the axial field of view of tomographs created with the introduced J-PET technology, while assuming angular acceptance cut on 45°.

6.2 J-PET technology vs. conventional PET systems

As shown in the Chapter 6.1, extension of the axial field of view is followed by the increase in sensitivity of the PET tomograph. In the standard PET scanners made with crystal scintillators such procedure is not easy to achieve because of the number of needed apparatus and huge costs. However, the J-PET technology simplifies this process by the utilization of very long plastic scintillator strips or few shorter strips (for example of length $\sim$ 50 cm), each stacked one after the other in the longitudinal direction and forming in total a ring structure. In order to inspect its prospects, the gain in the NEMA alike total sensitivity calculated from the 1st simulation type and presented in Figure 18a was estimated with respect to the state-of-the-art conventional short AFOV PET represented by the Biograph Vision. It was defined as a ratio

$$S_{tot}^{J-PET}(AFOV) \ / \ S_{tot}^{Biograph\ Vision} \tag{9}$$

between sensitivity of PET scanner of a given axial FOV and constructed with J-PET technology to sensitivity of the Biograph Vision. The study of the Biograph Vision scanner was performed in Chapter 5.4 during the Toy Monte-Carlo validation research. The value of the total sensitivity chosen for this analysis and equal to $S_{tot}^{Biograph\ Vision} = 5.809(76)$ [cps/kBq] was taken from the more accurate simulation with GATE software. The errors corresponding to every gain are statistical and calculated using the propagation of uncertainty technique. The obtained relation is shown in Figure 20.

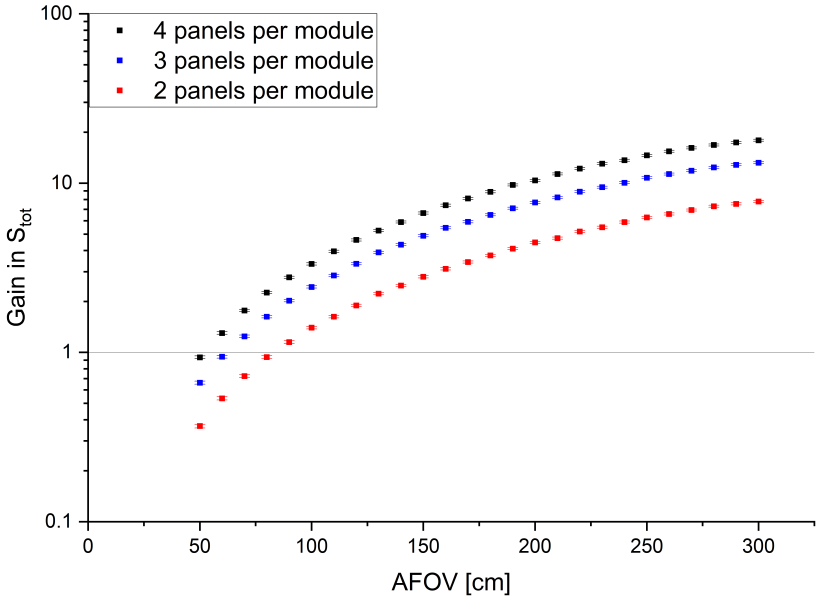

Figure 20: Gain in the total sensitivity of PET tomographs created using J-PET technology with respect to the state-of-art conventional PET system – Biograph Vision. A thin, black horizontal line situated at gain equal to 1 denotes the results comparable with conventional PET scanners.

The acquired results indicate that already $\sim$ 50 cm long geometry constructed from modules consisting of 4 panels provide comparable sensitivity to the conventional PET scanner from crystal scintillators. In case of other module types the field of view needs to be extended up to $\sim$ 90 cm. Nevertheless, such procedure is more accessible with J-PET systems and even in case of the two-layer module, the 200 cm AFOV gives $\sim$ 4.5 times gain. The most complex Total Body J-PET tomograph investigated in this thesis – 250 cm of field of view and 4 panels per module – can achieve almost 15 times better results with respect to the exemplary short FOV crystal PET. Moreover, the corresponding sensitivity at center, which can be interpreted as the sensitivity for point-like source, equal to $S_{center} = 124.1(1.0 \pm 1.1)$ [cps/kBq] (see Table 3) is slightly better than Biograph Vision's $S_{center} = 113.2(3.1)$ [cps/kBq] (see Table 7).

7 Sensitivity of the triple γ coincidence technique in the Total Body J-PET scanners

The principle of operation of standard positron emission tomography is based on the registration of two, back-to-back photons, originating from the e^+e^- annihilation event. The patient's body, or any other phantom material, provides only half of the needed particles – electrons. The second ingredient – positron, is introduced by the administration of radioisotope, which undergoes a $\beta+$ decay. Creation of the annihilation event and its further consequences were already described in detail in the Chapter 2.1. However, in many cases the $\beta+$ decay transforms the nuclei X into the excited state of the nuclei Y. As a result, an additional radiation is being emitted in the form of a, so-called, prompt photon of energy corresponding to the excitation energy. The prompt gamma carries extra information, which enables determination of the deexcitation moment. Since it occurs at a similar time as the quasi-stable positronium state is being formed, such knowledge provides a possibility for the positronium mean lifetime imaging [43, 50, 51, 52]. Nonetheless, this potential comes with a degradation in the sensitivity, because not two but three photons have to be registered in coincidence.

Therefore, a study of sensitivity with such triple γ coincidence technique were performed for each of the investigated Total Body J-PET systems. The introduced Toy Monte-Carlo model was chosen for the sake of simulations, as it allows for simple introduction of the prompt gamma. As described in the Chapter 5.2 the principle of operation of this approach can be described in four steps:

- Firstly, the z coordinate of the annihilation event is being simulated together with the direction of back-to-back emission. Because the prompt gamma originates in almost same place as 511 keV photons, there is only a need for simulation of additional direction of its flight.
- Secondly, the chance of interaction with a phantom material (if present) is being estimated. Since the phantom is the same for every of 3 gammas, the only addition is the value of linear attenuation coefficient for prompt photon in phantom's material.
- Next, the interaction with the scintillator is evaluated and similarly as previously, a new linear attenuation coefficient is required.
- Finally, a new selection efficiency criterion is needed.

The simulations were conducted assuming that ^{44}Sc isotope was chosen as a radioisotope. A corresponding reaction chain of $\beta+$ decay [53]:

$$^{44}Sc \rightarrow ^{44}Ca^* + e^+ + \nu \rightarrow ^{44}Ca + \gamma + e^+ + \nu$$

creates excited $^{44}Ca^*$ nucleus, which during the deexcitation process emits prompt photon of 1160 keV energy [43]. The values of linear attenuation coefficients for respective energy were assumed to be $\mu \equiv \mu_{Plastic} = 0.066$ cm^{-1} and $\mu_{phantom} \equiv \mu_{Water} = 0.066$ cm^{-1} [44]. The selection efficiency was estimated to 0.66, as a fraction of the energy deposition spectrum with deposited energy larger than the one from the 511 keV photons [43].

Sensitivity profiles of the triple γ true coincidences

Similarly as in the previously conducted research, two types of simulation were performed:

- with 2.5 meter radioactive source of 1 MBq activity,
- with additional 183 cm long water filled phantom.

Resulting sensitivity profiles are shown in Figure 21. Moreover, the numerical values of total sensitivities and sensitivities at center were estimated and are presented in Table 8. As expected, the improvement in the results with extension of the AFOV and increasing complexity of the module composition is preserved for the triple coincidence technique. Moreover, the uniform behavior over most of the phantom length (see Figure 21b) is still observable, especially for the 250 cm long geometries. Finally, the promising gain in sensitivity on the edges of the phantom is retained.

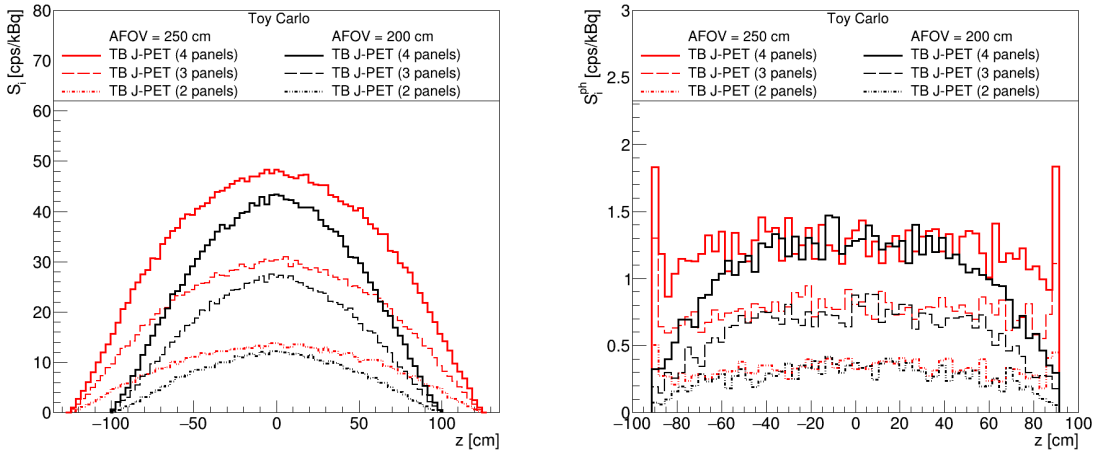

(a) Sensitivity profiles based on the simulation with a linear source.

(b) Sensitivity profiles based on the simulation with 183 cm long phantom.

Figure 21: Sensitivity profiles of the proposed Total Body J-PET tomographs using the triple γ coincidence technique.

Table 8: Total sensitivity and sensitivity at center of the proposed Total Body J-PET tomographs using the triple γ coincidence technique.

TB J-PET geometry		Simulation with source		Simulation with source & phantom	
Module	AFOV [cm]	S_{tot} [cps/kBq]	S_{center} [cps/kBq]	S_{tot}^{ph} [cps/kBq]	S_{center} [cps/kBq]
2 panels	200	5.69(02±07)	12.18(32±16)	0.26(01±02)	0.24(05±07)
3 panels	200	12.93(04±11)	26.94(48±21)	0.60(01±02)	0.88(09±10)
4 panels	200	20.80(01±02)	43.40(61±34)	1.02(01±04)	1.32(11±19)
2 panels	250	8.45(03±10)	13.82(34±28)	0.33(01±02)	0.32(05±06)
3 panels	250	19.02(04±10)	30.30(51±44)	0.77(01±02)	0.78(08±11)
4 panels	250	30.63(06±31)	48.37(64±60)	1.24(01±05)	1.37(11±17)

Due to the fact, that the prompt gamma is emitted isotropically and do not posses any related companion (as in case of back-to-back photons), the geometrical acceptance for its registration is much higher than for the 511 keV photons. It is not limited by the condition that the second photon flying in the opposite direction has to intersect with the tomograph in order to have a chance for detection. Therefore, the angular acceptance criterion wasn't introduced in this study. It requires a dedicated detailed research, which is not possible to perform with the introduced in this thesis Toy Monte-Carlo model.

Dependence on the axial field of view

Furthermore, the dependence of the triple γ coincidence sensitivity on the axial field of view of PET tomographs based on the J-PET technology was investigated. For this purpose the values of S_{tot} and S_{center} were calculated using the first presented, NEMA-like type of simulation. The obtained relations are presented in Figures 22a and 22b. The slightly accelerating behavior up to the source length described in the Chapter 6.1 is still visible for the total sensitivity. However, in case of the S_{center}, previous decrease in the relation growth (for double γ coincidence) is weaker.

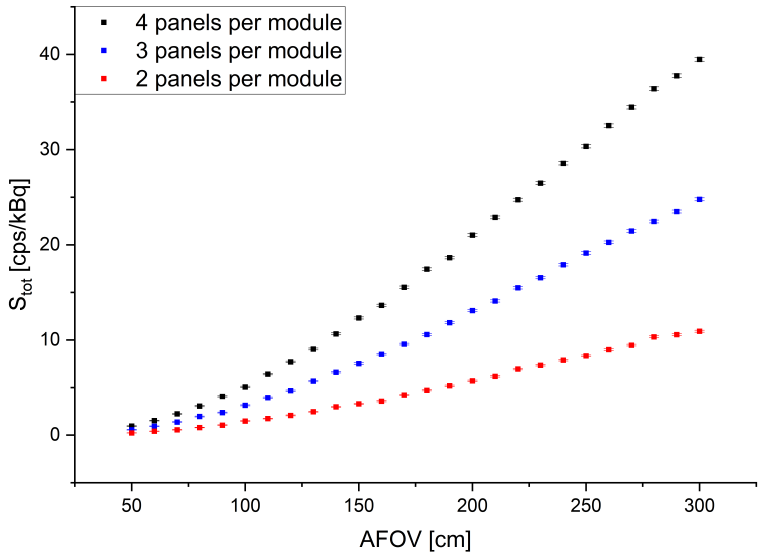

(a) Dependence of total sensitivity on AFOV.

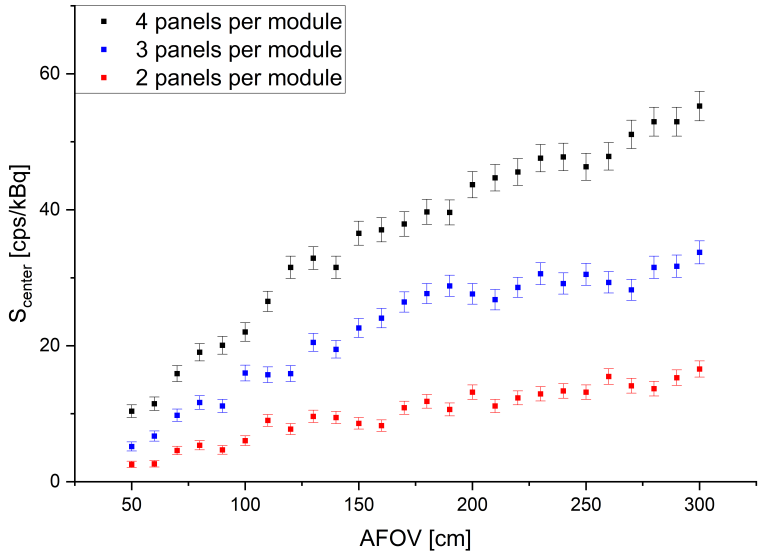

(b) Dependence of sensitivity at center on AFOV.

Figure 22: The dependence of sensitivity on the axial field of view of tomographs created with the introduced J-PET technology for triple γ coincidence technique.

Triple coincidence technique in relation to the standard methods

The triple γ coincidence technique in its assumption causes degradation in the achievable sensitivity of PET tomographs, while enabling the positronium mean lifetime imaging. In order to inspect its degrading influence, a comparison with the standard double γ technique was performed with the NEMA alike total sensitivity parameter. The results of the latter method were already presented in Figure 18a. The acquired relation is shown in Figure 23, where it is presented in a form of gain denoted as a ratio

$$S^{2\gamma}_{tot}(AFOV)/S^{3\gamma}_{tot}(AFOV)\ . \tag{10}$$

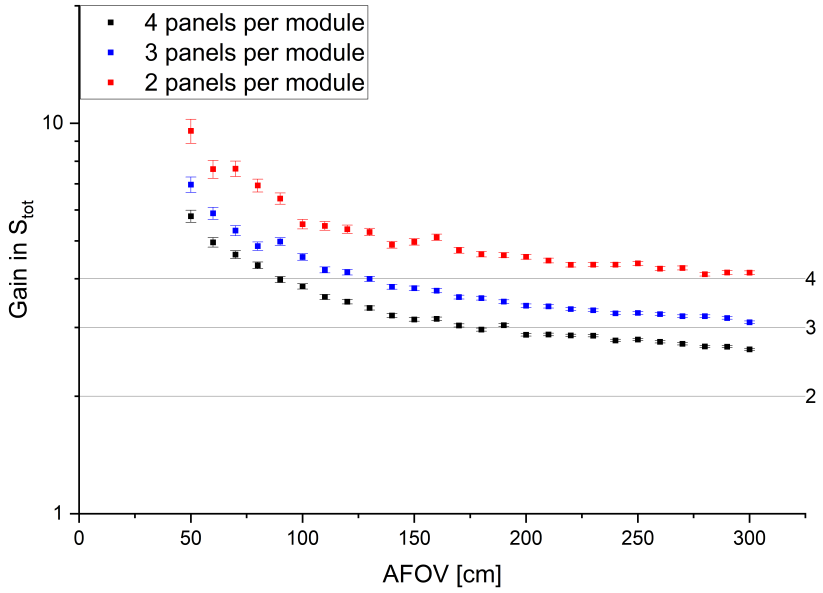

Figure 23: Total sensitivity of J-PET tomographs between double and triple γ coincidence technique.

The errors corresponding to every gain are statistical and calculated using the propagation of uncertainty technique. Results indicate that there is a descending trend in gain between both coincidence methods, which slows down for higher axial fields of view. Moreover, utilization of modules constructed with higher number of panels has a favorable influence on reducing of gain. For the most complex of investigated Total Body J-PET systems, the triple coincidence technique is only ~ 3 times worse than standard technique.

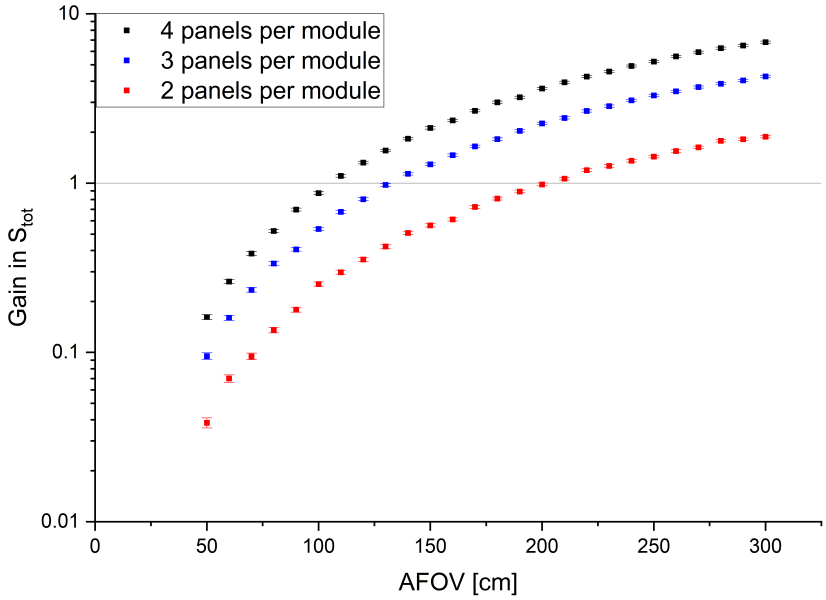

Figure 24: Gain in the triple γ coincidence total sensitivity of J-PET tomographs with respect to the Biograph Vision system. A thin, black horizontal line situated at gain equal to 1 denotes the results comparable with conventional PET scanners.

Finally, also the gain with respect to the conventional tomograph represented by the Biograph Vision, which utilizes double γ technique was estimated (following Equation 9). The obtained results are presented in Figure 24. While in comparison to the double coincidence method the inspected one gives few times worse results, they are still better than of conventional PET system. Even the least complex of six introduced Total Body J-PET variants starts to improve the total sensitivity obtained by the clinically used PET tomographs.

8 Summary and conclusions

The main aim of this thesis was to investigate sensitivity of the Total Body PET tomographs proposed by the Jagiellonian PET Collaboration [1, 2, 3, 4]. For this purpose a simulation-based study was performed with the use of the GATE software [11, 12, 13, 14]. Additionally, a Toy Monte-Carlo model was developed as a simplified approach to the sensitivity study. Its concept is based on the fact that emission of the back-to-back photons during the annihilation event is isotropic. Together with the axially symmetric cylindrical geometry of PET scanner, this allows for simplification of Positron Emission Tomography simulations into only 2 dimensions. Simulation of each event can be then described with only z coordinate of annihilation and the polar angle of emission. Next, each annihilation photon is carefully tracked and its interactions with matter are calculated, which leads to the determination of detection position. However, the exact values of energy depositions are not taken into account. Instead, they are replaced with a new selection efficiency coefficient determined separately for each scintillator material.

Introduced Toy Monte-Carlo model was checked and validated by a comparison with GATE software for PET tomographs constructed with organic and inorganic scintillators. Its applicability for conventional short axial field of view scanners, as well as Total Body systems was proven. Moreover, the possibility of simulating sparse geometries was also shown.

The results of sensitivity for six Total Body J-PET variants were calculated as numerical values and the sensitivity profiles. Additionally, the influence of inner construction of tomograph was studied. Furthermore, also a dependence of the sensitivities on a vast range of axial fields of view were examined and compared to the conventional, short field of view PET system. The obtained results show that the standard imaging total sensitivity achievable with the Total Body PET tomographs designed using the J-PET technology equals to 25.92(05±04) [cps/kBq] for the 2 meter long two-layer tomograph and 84.74(0.9±1.1) [cps/kBq] for the 2.5 meter long four-layer tomograph. They exceed the conventional PET systems (represented by the Biograph Vision) by a factor of ~ 4.5 and ~ 15 respectively. Moreover, they provide almost uniform simultaneous sensitivity over the whole patient with the sensitivity at the center of the tomograph reaching up to 124.1(1.0±1.1) [cps/kBq]. Study of the dependence of the sensitivity at center on the tomograph's length indicates that the initial increase slows above ~ 100 cm and above ~ 200 cm is almost negligible.

Since the Total Body systems create new challenges in image reconstruction like parallax error or registration of highly attenuated photons, the influence of the angular acceptance criterion [42] on the sensitivity was assessed for all six simulated J-PET systems. For that purpose, a simulation consisting of a radioactive source placed within a water filled phantom, which mimics the influence of a human body was performed. Achieved maximal total sensitivity was estimated to 7.94(11±45) [cps/kBq] and sensitivity at center to 8.66(86±90) [cps/kBq]. Following application of the 45 degree angular acceptance criterion resulted with ∼11% (∼25%) reduction of the total sensitivity and ∼18% (∼18%) of sensitivity at center for 200 cm (250 cm) long Total Body J-PET tomographs.

Finally, the sensitivity for the novel positronium mean lifetime imaging [43, 50, 51, 52] was examined. The obtained total sensitivity equal up to 30.63(06±31) [cps/kBq] proved to again outperform the conventional PET systems by ~ 5 times, whilst featuring uniform sensitivity along the patient's body with 48.37(64±60) [cps/kBq] sensitivity at center.

References

[1] P. Moskal, E. Ł. Stępień, *Prospects and Clinical Perspectives of Total-Body PET Imaging Using Plastic Scintillators*, PET Clin., Vol. 15, no. 4, pp. 439-452, 2020

[2] S. Niedźwiecki et al., *J-PET: A New Technology for the Whole-body PET Imaging*, Acta Phys. Pol. B, Vol. 48, no. 10, pp. 1567-1576, 2017

[3] P. Moskal, P. Kowalski, R. Y. Shopa, L. Raczyński et al., *Simulating NEMA characteristics of the modular total-body J-PET scanner – an economic total-body PET from plastic scintillators* , Phys Med Biol., Vol. 66, 175015, 2021

[4] Jagiellonian PET Collaboration web page
URL address: http://koza.if.uj.edu.pl/pet/
Access date: 24.07.2021

[5] World Health Organization, *WHO report on cancer: setting priorities, investing wisely and providing care for all*, World Health Organization, 2020

[6] S. R. Cherry, T. Jones, J. S. Karp, J. Qi, W. W. Moses and R. D. Badawi, *Total-Body PET: Maximizing Sensitivity to Create New Opportunities for Clinical Research and Patient Care*, J. Nucl. Med., Vol. 59, no. 1, pp. 3-12, 2018

[7] S. Vandenberghe, P. Moskal and J. S. Karp, *State of the art in total body PET*, EJNMMI Phys., 7:35, 2020

[8] P. Moskal et al., *Potential of the J-PET Detector for Studies of Discrete Symmetries in Decays of Positronium Atom — A Purely Leptonic System*, Acta Phys. Pol. B, Vol. 47, no. 2, pp. 509-535, 2016

[9] B. C. Hiesmayr and P. Moskal, *Witnessing Entanglement In Compton Scattering Processes Via Mutually Unbiased Bases*, Sci Rep, 9:8166, 2019

[10] B. C. Hiesmayr and P. Moskal, *Genuine Multipartite Entanglement in the 3-Photon Decay of Positronium*, Sci Rep, 7:15349, 2017

[11] D. Sarrut et al., *Advanced Monte Carlo simulations of emission tomography imaging systems with GATE*, Phys Med Biol., Vol. 66, no. 10, 2021

[12] S. Jan, G. Santin, D. Strul et al., *GATE: a simulation toolkit for PET and SPECT*, Phys. Med. Biol., Vol. 49, Issue 19, pp. 4543-4561, 2004

[13] S. Jan, D. Benoit, E. Becheva et al., *GATE V6: a major enhancement of the GATE simulation platform enabling modelling of CT and radiotherapy*, Phys. Med. Biol., Vol. 56, Issue 4, pp. 881-901, 2011

[14] D. Sarrut, M. Bardiès, N. Boussion et al., *A review of the use and potential of the GATE Monte Carlo simulation code for radiation therapy and dosimetry applications*, Med. Phys., Vol. 41, Issue 6, 2014

[15] J. Allison et al., *Recent Developments in Geant4*, Nucl. Instrum. Meth. A, Vol. 835, pp. 186-225, 2016

[16] J. Allison et al., *Geant4 Developments and Applications*, IEEE Trans. Nucl. Sci., Vol. 53, Issue 1, pp. 270-278, 2006

[17] S. Agostinelli et al., *Geant4 - A Simulation Toolkit*, Nucl. Instrum. Meth. A, Vol. 506, Issue 3, pp. 250-303, 2003

[18] P. Moskal, P. Salabura, M. Silarski, J. Smyrski, J. Zdebik and M. Zieliński, *Novel Detector Systems for the Positron Emission Tomography*, Bio-Algorithms and Med-Systems, Vol. 7, no. 2, pp. 73–78, 2011

[19] M. Pawlik - Niedźwiecka, *Studies of changes of signals shapes in plastic scintillator strips*, MA Thesis, Jagiellonian University, Kraków, 2014

[20] M. E. Phelps, S. R. Cherry and M. Dahlbom, *PET: Physics, Instrumentation, and Scanners*, Springer, 2006

[21] D. L. Bailey, D. W. Townsend, P. E. Valk and M. N. Maisey (Eds), *Positron Emission Tomography Basic Sciences*, Springer, 2005

[22] D. A. Rich, *A Brief History of Positron Emission Tomography*, J. Nucl. Med. Technol., Vol. 25, no. 1, pp. 4-11, 1997

[23] H. N. Wagner Jr, *A brief history of positron emission tomography (PET)*, Semin Nucl Med., Vol. 28, Issue 3, pp. 213-220, 1998

[24] M. M. Ter-Pogossian, *The origins of positron emission tomography*, Semin Nucl Med., Vol. 22, Issue 3, pp. 140-149, 1992

[25] E. Czaicka, *Liniowy model pozytonowego tomagrafu emisyjnego*, MA Thesis, Jagiellonian University, Kraków, 2008

[26] P. Moskal, Sz. Niedźwiecki et al., *Test of a single module of the J-PET scanner based on plastic scintillators*, Nuclear Instruments and Methods in Physics Research Section A: Accelerators, Spectrometers, Detectors and Associated Equipment, Vol. 764, pp. 317-321, 2014

[27] P. Kowalski, W. Wiślicki, L. Raczyński et al., *Scatter fraction of the J-PET tomography scanner*, Acta Phys. Pol. B, Vol. 47, Issue 2, pp. 549–560, 2016

[28] National Electrical Manufacturers Association, *NEMA Standards Publication NU 2-2018*, National Electrical Manufacturers Association, 2018

[29] M. Watanabe et al., *A high-throughput whole-body PET scanner using flat panel PS-PMTs*, IEEE Trans. Nucl. Sci., Vol. 51, no. 3, pp. 796–800, 2004

[30] M. Conti et al., *Performance of a high sensitivity PET scanner based on LSO panel detectors*, IEEE Trans. Nucl. Sci., Vol. 53, no. 3, pp. 1136–1142, 2006

[31] S. Surti, A. R. Pantel and J. S. Karp, *Total Body PET: Why, How, What for?*, IEEE Transactions on Radiation and Plasma Medical Sciences, Vol. 4, no. 3, p. 283-292, 2020

[32] EXPLORER PET Consortium web page
URL address: https://explorer.ucdavis.edu/
Access date: 24.07.2021

[33] Biograph Vision Quadra from the Siemens Healthineers web page
URL address:
https://www.siemens-healthineers.com/molecular-imaging/pet-ct/biograph-vision-quadra
Access date: 24.07.2021

[34] M. A. Akl, O. Bouhali, Y. Toufique, J. S. Karp and S. Vandenberghe, *Monte Carlo sensitivity study of a long axial FOV PET scanner with patient adaptive rings*, IEEE Nuclear Science Symposium and Medical Imaging Conference (NSS/MIC), pp. 1-3, 2019

[35] S. Vandenberghe et al., *PET20.0: a cost efficient, 2mm spatial resolution Total Body PET with point sensitivity up to 22% and adaptive axial FOV of maximum 2.00m*, http://hdl.handle.net/1854/LU-8582525

[36] R. D. Badawi, H. Shi, P. Hu, S. Chen, T. Xu, P. M. Price, Y. Ding, B. A. Spencer, L. Nardo, W. Liu, J. Bao, T. Jones, H. Li and S. R. Cherry, *First Human Imaging Studies with the EXPLORER Total-Body PET Scanner**, J. Nucl. Med., Vol. 60, no. 3, pp. 299-303, 2019

[37] J. S. Karp, V. Viswanath, M. J. Geagan, G. Muehllehner, A. R. Pantel, M. J. Parma, A. E. Perkins, J. P. Schmall, M. E. Werner and M. E. Daube-Witherspoon, *PennPET Explorer: Design and Preliminary Performance of a Whole-Body Imager*, J. Nucl. Med., Vol. 61, no. 1, pp. 136-143, 2020

[38] A. R. Pantel, V. Viswanath, M. E. Daube-Witherspoon, J. G. Dubroff, G. Muehllehner, M. J. Parma, D. A. Pryma, E. K. Schubert, D. A. Mankoff and J. S. Karp, *PennPET Explorer: Human Imaging on a Whole-Body Imager*, J. Nucl. Med., Vol. 61, no. 1, pp. 144-151, 2020

[39] P. Kowalski et al., *Estimating the NEMA characteristics of the J-PET tomograph using the GATE package*, Phys. Med. Biol., Vol. 63, no. 16, 2018

[40] J. Smyrski, D. Alfs, T. Bednarski et al., *Measurement of gamma quantum interaction point in plastic scintillator with WLS strips*, Nuclear Instruments and Methods in Physics Research A, Vol. 851, Issue 5, pp. 39–42, 2017

[41] GATE's documentation
URL address: https://opengate.readthedocs.io/en/latest/index.html
Access date: 24.07.2021

[42] M. Dadgar , S. Parzych, F. Tayefi Ardebili , *A simulation study to estimate optimum LOR angular acceptance for the image reconstruction with the Total Body J PET*, Lecture Notes in Computer Science, Vol. 12722, pp. 189-200, 2021

[43] P. Moskal, D. Kisielewska, R. Y. Shopa et al., *Performance assessment of the 2γ positronium imaging with the total-body PET scanners*, EJNMMI Phys., 7:44, 2020

[44] National Institute of Standards and Technology
URL address: https://www.nist.gov/pml
Access date: 24.07.2021

[45] R. Barlow, *Systematic errors: Facts and fiction*, 2002, arXiv:hep-ex/0207026

[46] Biograph Vision from the Siemens Healthineers web page
URL address:
https://www.siemens-healthineers.com/molecular-imaging/pet-ct/biograph-vision
Access date: 24.07.2021

[47] B. A. Spencer et al., *Performance Evaluation of the uEXPLORER Total-Body PET/CT Scanner Based on NEMA NU 2-2018 with Additional Tests to Characterize PET Scanners with a Long Axial Field of View*, J Nucl Med., Vol. 62, Issue 6, pp. 861-870, 2021

[48] É. Gaudin, M. Toussaint, C. Thibaudeau, M. Paillé, R. Fontaine and R. Lecomte, *Performance Simulation of an Ultrahigh Resolution Brain PET Scanner Using 1.2-mm Pixel Detectors*, IEEE Transactions on Radiation and Plasma Medical Sciences, Vol. 3, no. 3, pp. 334-342, 2019

[49] Y. Toufique, O. Bouhali, P. Negre et al., *Simulation study of a coincidence detection system for non-invasive determination of arterial blood time-activity curve measurements*, EJNMMI Phys., 7:25, 2020

[50] P. Moskal, D. Kisielewska, et al., *Feasibility study of the positronium imaging with the J-PET tomograph*, Phys Med Biol., Vol. 64, no. 5, 2019

[51] P. Moskal et al., *TOF-PET tomograph and a method of imaging using a TOF-PET tomograph, based on a probability of production and lifetime of a positronium*, Patent US 9851456, PL 227658 (2013). 2017

[52] K. Dulski et al., *Analysis procedure of the positronium lifetime spectra for the J-PET detector*, Acta Phys Pol. A, Vol.132, Issue 5, pp. 1637-1640, 2017

[53] M. Sitarz, JP. Cussonneau, T. Matulewicz, F. Haddad, *Radionuclide candidates for $\beta + \gamma$ coincidence PET: An overview*, Appl Radiat Isot., Vol. 155, 2020